Image Restoration with Multiple Directional Transforms

A Dissertation
in
Electrical and Information Engineering
Submitted to Graduate School of Science and Technology
Niigata University
in
Partial Fulfillment of the Requirements
for the Degree of
Doctor of Philosophy

Zhiyu Chen
August, 2015

Contents

Abstract

This thesis deals with the application of multiple directional transforms to image restoration, and discusses two cases of image restoration, image denoising and image fusion.

In Chapter 1, the background of image restoration is described. First, image denoising problems are addressed. Image denoising is a principal problem of image processing and the purpose is to obtain an original picture as an ideal one. For photon acquisition systems, low-light image denoising is becoming in use in optical imaging applications such as astronomical imaging, fluorescence microscopy appliances, magnetic resonance imaging. In this case, the noises are strongly dependent on the signals and approximately obeys Poisson distribution, which leads difficulties in denoising process. The denoising problem for Poisson noise can be modeled by a modular fashion through variance stabilization. Using the variance stabilization, denoising techniques for additive Gaussian noises become available for Poisson denoising. This chapter summarizes some of such existing methods.

Next, image fusion problems are dealt with. Image fusion is a technique to synthesize a full focused picture, in which all the contents are focused, from a set of partially focused images with different focal lengths. At present, there are several types of image fusion techniques. Those include spatial domain, feature space and transform domain techniques. In the spatial domain and feature space approaches, the synthesis performance heavily depends on the adopted segmentation algorithm, and they prone to fail fusion at object edges, while the transform domain approach is influenced by the adopted transform. In order to improve the quality of fused image, some disadvantages of existing methods are discussed in this chapter.

This chapter mentions the possibility of improving the performance of Poisson denoising and image fusion from viewpoints different form existing researches.

In Chapter 2, from comparison with Discrete Cosine Transform (DCT) and Discrete Wavelet Transform (DWT), the features of directional lapped orthogonal transforms (DirLOTs) are discussed and emphasized For preparation of Chapter 3 and later, explanations on DirLOTs are given through some figures and expressions. Based on the relationship between directivity of DirLOT and slant edge and texture of image, the possibility of the performance improvement of image restoration is described.

In Chapter 3, a Poisson denoising method is proposed. Various discrete wavelet transforms have been used for Poisson image denoising. However, the transforms have disadvantages such as shift variance, aliasing, and lack of directional selectivity. PURE-LET is known as an efficient Poisson denoising

technique. However, PURE-LET has a disadvantage of representing slant geometric structures. As another method, there is a technique to convert Poisson noise to additive Gaussian noise so that typical Gaussian denoising technique becomes available. Among many Gaussian denoising methods, the SURE-LET approach is known to be relatively efficient. SURE-LET is a kind of soft-thresholding method that uses a relation among inter-scale coefficients of an orthonormal wavelets. Its performance, however, depends on the adopted wavelets. Classical separable transforms bring poor representation of slant edges and textures. In order to solve this problem, this section proposes to combine the variance stabilizing transformation (VST), SURE-LET approach and multiple DirLOTs (M-DirLOTs). Experimental results show that the proposed method is able to significantly improve the denoising performance.

In Chapter 4, an image fusion method is proposed. Image fusion is a scheme to improve the quality of information from multiple images. This chapter deals with an image fusion technique in wavelet transform domain. Some wavelet-based algorithms were developed. For more effective representation of image, we use multiple directional transforms to fuse images. M-DirLOTs can overcome a disadvantage of traditional separable wavelets for representing slant textures and edges of images. This work analyses characteristics of local luminance contrast and suggests a novel fusion rule based on inter-scale relation of wavelet coefficients. Relying on the above consideration, a novel image fusion method based on inter-scale relation in M-DirLOTs domain is proposed. Some experimental results show that the proposed method improves the fusion performance.

In Chapter 5, conclusions of this thesis and future works are summarized.

Index Terms– Poisson noise, Multiple directional transform, Image fusion, Luminance contrast, Interscale relation

Acknowledgements

Acknowledgements My deepest gratitude goes first and foremost to advisory professors Dr. Shogo Muramatsu, for his constant encouragement and guidance. He has walked me through all the stages of the writing of this thesis. He has given me lots of useful advices on my writing, and has tried his best to improve this thesis. Second, I would like to express my heartfelt gratitude to Professors Dr. Hisakazu Kikuchi, Dr. Shigenobu Sasaki, Dr. Masahiro Yukawa and Dr. Masanobu Yamamoto, who have instructed and helped me a lot in the past three years. Without their consistent and illuminating instructions, this thesis could not have reached its present form.

I would like to acknowledge the support from JSPS KAKENHI Grant Number 26420347, and from the other members of the KLab. Although there have appeared no names here, I thank to all individuals in Department of Electrical and Information Engineering and Graduate School of Science and Technology, Niigata University.

Last but not the least, my thanks would go to my beloved family for their loving considerations and great confidence in me all through these years. I also owe my sincere gratitude to my friends who gave me their help and time in listening to me and helping me work out my problems during the difficult course of the thesis.

July, 2015
Zhiyu Chen

1 Introduction

In a time of Information Revolution, we receive and exchange information all the time. High quality display images are becoming in use in consumer appliances, e.g., astronomical imaging, fluorescence microscopy appliances, and medical instruments. An image acquisition system should take a photo which has enough definition for detecting and analysing objects even under inferior conditions. For that reason, image restoration such as denoising, deblurring, super-resolution, inpainting and enhancement are applied in image processing applications. In order to solve these problems, we proposes to apply multiple DirLOTs (M-DirLOTs) to image restoration. In this thesis, we deal with image denoising and image fusion.

1.1 Poisson Image Denoising

Image denoising is one of basic problems in image processing. The purpose is to make the quality of noisy image better. Measurement noise is possible to occur in digital image acquisition, where the predominant source is the stochastic nature of the photon-counting process at the detectors [1], [2]. Under some conditions such as low-power light source, short exposure time, and phototoxicity appeared in the photon acquisition systems (e.g., fluorescence microscopy, astronomy and medical devices), only a few photons are collected by the photosensors, producing noise that approximately obeys Poisson distribution. Poisson noise strongly depends on signals, leading to difficulties in the denoising process. During the image denoising, the noise corrupted by the source mentioned above can be modeled as Poisson noise [3], [4], [5].

The denoising problem for Poisson noise can be modeled by a modular fashion through variance stabilization [6], [7]. The variance of Gaussian noise is stationary, whereas the variance of Poisson noise is non-stationary. It is possible to describe the denoising process as follows: First, to modify the noisy data, a nonlinear variance stabilizing transformation (VST) is applied. Second, to treat the modified noisy data, algorithms designed for removing Gaussian noise is applied. Third, to obtain the desired estimation of the unknown noise-free image, an inverse VST is applied to the denoised data. Fig.1.1 shows the

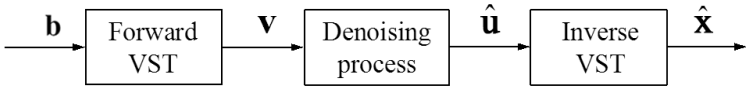

Figure 1.1: Poisson denoising method based on VST.

Poisson denoising method based on VST, where $\mathbf{b}$, $\mathbf{v}$, $\hat{\mathbf{u}}$ and $\hat{\mathbf{x}}$ are image contaminated by the Poisson noise, transformed data, denoised data and inverted image, respectively.

In the first step, since the image is corrupted by the signal-dependent noise whose variance varies with the expectation of the pixel value, the VST should be applied so that the transformed data of Poisson noise can be approximately modeled by the Gaussian noise distribution with a constant variance [5], [6], [7]. It becomes possible to apply a denoising process for Gaussian noise algorithms to Poisson denoising.

Among Gaussian denoising methods, the SURE-LET approach with an orthonormal wavelet transform is relatively efficient [8]. The SURE-LET is a one-pass denoising algorithm and involves only simple thresholding operations in wavelet domain. However, its performance becomes worse for the regions where the interscale correlation is weak. Furthermore, diagonal textures, edges and gradation are inadequately represented with separable transforms (e.g., Haar and Symlets). As well, some Poisson denoising methods have been developed so far. A denoising algorithm designed for Poisson noise based on a Haar-Fize transform has been proposed in [4]. The Haar-Fize transform cannot satisfy directional characteristics. Zhang et al. proposed a hybrid approach that combines VSTs, hypothesis testing, l_1-penalized restoration and advanced redundant multiscale representations [9]. In [2], minimizing MSE estimation for Poisson noise based on an unnormalized Haar wavelet transform, so called PURE-LET, was proposed. PURE-LET is very efficient in terms of denoising performance and computational complexity. PURE-LET exploits a linear denoising function to search the optimal solution. However, the adopted wavelet transform has a disadvantage of representing diagonal geometric structures. At present, block-matching and 3D filtering (BM3D), which is based on sparse 3D transform-domain collaborative filtering, is frequently referenced as the state-of-the-art [10]. The BM3D can achieve an excellent denoising result. The computation, however, is relatively complex and the one-pass thresholding implementation is principly impossible.

1.2 Multi-focus Image Fusion

As known, the focused range of visible imaging system is limited. Thus, it is difficult to obtain all objects in the same scene clearly. A well-focused image has clearer detail than a defocused image comparatively. To acquire a focused image is a basic task for human perception and machine vision. Image fusion is a scheme to improve the quality of information from a set of images. The image fusion is the process of combining relevant information from multiple images into a single image. The fused image will be more informative than

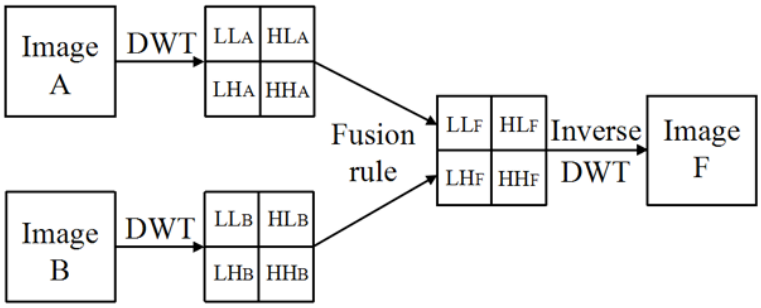

Figure 1.2: Image fusion framework based on DWT.

any of the original images. More reliable and accurate information can be provided by the image fusion with multi-sensor data. Multiple images which are captured at different focus levels are used to reconstruct a single image in the approach proposed in the article [11]. It is basically realized by combining well-focused clear parts of multiple source images. Image fusion of multiple images will increase the image quality.

At present, there are mainly two approaches in multi-focused image fusion. One approach selects pixels from all clear parts of source images in the spatial domain or feature space to produce a fused image. However this approach causes blocking effect, which has great influence on the quality of fused image. Moreover, this approach hardly depends on the adopted segmentation algorithm, making the choice serious. For instance, if an object in a source image is partially clear and blur, an object will be extracted from the source image with the blur part when the whole of the object needs to be considered in the segmentation algorithm [12], [13].

The other approach achieves the fusion from coefficients of multi-scale transform under a premise that the detailed information of image is distributed in high frequency subbands. It is known that Discrete Cosine Transform (DCT), Discrete Wavelet Transform (DWT), Dual-Tree Complex Wavelet Transform (DT-ℂWT), Curvelet and Contourlet can be used as the transform [14]. A framework of an image fusion system is shown in Fig.1.2 [15]. The inherent feature of the wavelet transform provides the following advantages:

1. Perfect restoration property which ensures no information loss in the signal decomposition process.
2. Decomposition of an image into the approximation and detail image, which represents the different structure of the original image.
3. The decomposition tiling of the 2-D DWT matches to the human visual system.

In [14], wavelet multi-resolution decomposition has been applied to coefficient-level image fusion. Based on this method, a shift-invariant wavelet was mentioned to improve the fusion quality [15]. Some wavelet-based algorithms were developed in the articles [16] and [17]. However, the wavelet transform has characteristics in limited directions. A new construction, sharp frequency localization Contourlet transform (SFLCT), was suggested in [18]. In some studies, the authors indicate the method can alleviate the problem of non-localization. However, it causes pseudo-Gibbs phenomena easily. In order to overcome these disadvantages, Cycle Spinning was proposed [19]. Some multi-focus image fusion methods based on non-subsampled contourlet transform (NSCT) have been proposed [20], [21]. NSCT can lead to better frequency selectivity and regularity, but the computational complexity is high. Based on non-subsampled shearlet transform (NSST), a multi-focus image fusion method was proposed [22]. Although the image fusion performance for diagonal textures and edges was improved, there remains a disadvantage that the NSCT and NSST cannot satisfy orthogonality, and the computational complexity is still high. In [23], a fusion method based on DT-$\mathbb{C}$WT was introduced.

1.3 Problem Statement

In practical applications, all kinds of wavelet transforms have been evolved and shown the ability in representing natural images that contain smooth areas separated with edges. However, natural images consist of edges that are smooth curves, which cannot be captured efficiently by these transforms. To overcome some shortcomings of traditional transforms, the dual-tree complex wavelet transform (DT-$\mathbb{C}$WT) was proposed [24]. The 2-D DT-$\mathbb{C}$WT have six subbands that give information about the details of an image, where the angles are set to $\pm 15, \pm 45, \pm 75$ degrees. Note that the DT-$\mathbb{C}$WT has only fixed directions for choice. Since the construction is based on real 1-D two-channel filter banks, the design and implementation are not complicated. However, the structure is restrictive. For example, the symmetric and orthogonal property are not simultaneously satisfied. The curvelet is one of the successful 2-D transforms, which can efficiently approximate smooth curve edges [25]. There is a question how to construct a tight curvelet-like transform in discrete domain. In [26], Do and Vetterli start with discrete-domain construction of filter banks for producing an alternative directional multiresolution analysis framework (Contourlet transform). In order to solve pseudo-Gibbs phenomena, NSCT was proposed [27]. However, these frameworks are also restrictive to satisfy both of tightness and symmetry simultaneously. A non-subsampled shearlet transform (NSST) was proposed [28]. NSST can capture

two-dimensional geometrical structure much more effectively than traditional multi-scale transform. There remains a disadvantage that the NSST cannot satisfy orthogonality, and the computational complexities are high.

In the above transforms, the orthogonality, symmetry, overlapping and directionality cannot be achieved at the same time. For more effective representation of image, we proposed a new transform, M-DirLOTs, using non-separable and directional filter banks that can efficiently represent images containing contours, textures and gradation with few coefficients [29]. M-DirLOTs are not only with multi-scale, but also with multi-direction property. Compared with the traditional transforms, M-DirLOTs can represent edges and other singularities along trend surfaces much more efficiently. In order to improve the image restoration performance, we apply M-DirLOTs to Poisson denoising and image fusion.

1.4 Organization

This section shows the organization of this thesis. This thesis mainly consists of two parts. The first part deals with the problem of the Poisson noise removal. The other part discusses multi-focus image fusion. This dissertation considers image denoising and image fusion. In this thesis, we propose to apply a union of directional lapped orthogonal transforms (DirLOTs) to image restoration problems. DirLOTs are 2-D non-separable lapped orthogonal transforms with directional characteristics. Its bases overcome a disadvantage of separable transforms and suitable for restoring slant textures and edges in images. Based on this feature, multiple DirLOTs are first applied to construct multi-scale representations and then unified to construct a redundant dictionary so that the restoration performance is improved. Experimental results show that the unified dictionary of multiple multi-scale DirLOTs is able to significantly improve the performance of image restoration. This thesis is organized as follows:

Chapter 2: Multi-directional Transform

In Chapter 2, the multi-scale transform are reviewed. Their features are described.

Chapter 3: Heuristic Poisson Denoising with M-DirLOTs

In Chapter 3, Heuristic Restoration will be introduced. Firstly, we analyse the Poisson noise model with its important features and properties. The process is difficult to Poisson denoising, since the noise strongly depend on signals. Meanwhile, the denoising results depend on wavelet transform. In order

to improve the Poisson denoising result, we propose a method based on multiple directional transforms. The denoising results confirm that the approach is very competitive to some state-of-the-art denoising methods. A classical VST and state-of-the-art Gaussian denoising algorithm (SURE-LET) are introduced. The combination of VST, SURE-LET and M-DirLOTs is proposed to reduce Poisson noise. The denoising results confirm that the approach is very competitive to some state-of-the-art denoising methods.

Chapter 4: Heuristic Image Fusion with M-DirLOTs

In Chapter 4, an image fusion framework with DWT. Image fusion is a scheme to improve the quality of information from multiple images. For more effective representation of image, we use multiple directional transforms to fuse images. We investigate features of the local luminance contrast. An influential review of the related work on imgae fusion is provided. A new measurement based on interscale relation of wavelet coefficients is proposed to fuse image. Several experimental results are presented. Common measurements apply to evaluate the performance of denoising and fusion approaches. Several state-of-the-art approaches are described and compared to each other in details. Both objective and subjective image quality assessments are discussed.

Chapter 5: Conclusions and Future Work

In Chapter 5, some conclusions is summarized and potential future work is shown.

2 Multi-directional Transform

In this chapter, we detail the basic concepts of multi-directional transform. The general purpose of most signal processing applications is to decompose an original signal into a primitive or fundamental constituents, and to perform simple operations separately on each components, in order to accomplish sophisticated operations via a combination of several divided operations. In recent years, multi-directional transforms have been supplemented by many new ideas. These alternatives aim to provide more useful ways for analyzing and processing signals in different applications, but the classic methods still act as a useful theoretical tool for evaluating the new one and still dominate the discussion.

2.1 Discrete Cosine Transform

A discrete cosine transform(DCT) describes a sequence of finitely many points in terms of a sum of cosine functions oscillating at different frequencies. DCT is essential in numerous applications of science and engineering, because it has a strong energy compaction property. After decorrelation the image data with DCT, each transform coefficient can be encoded independently without losing compression efficiency. And this reveals some of the vital characters of DCT.

The most common DCT definition of a 1-D sequence of length M is

$$C(n) = \sum_{n=0}^{M-1} \sqrt{\frac{2}{M}} c_k \cos \frac{k(n+\frac{1}{2})\pi}{M}, \ k = 0, 1, ..., M-1,$$

where c_k is defined as

$$c_k = \begin{cases} \frac{1}{\sqrt{2}} & k = 0 \\ 1 & k = 1, 2, ..., M-1. \end{cases}$$

This makes DCT matrix orthogonal. The construction of 2-D DCT is based on the definition of 1-D.

2.2 Discrete Wavelet Transform

The discrete wavelet transform(DWT) linear map data from the time domain to the wavelet domain. This decomposition is repeated to increase the frequency resolution and the approximation coefficients decomposed by high and low pass filters. It is represented as a binary tree with nodes representing a sub-space with a different time-frequency localization. The tree is shown

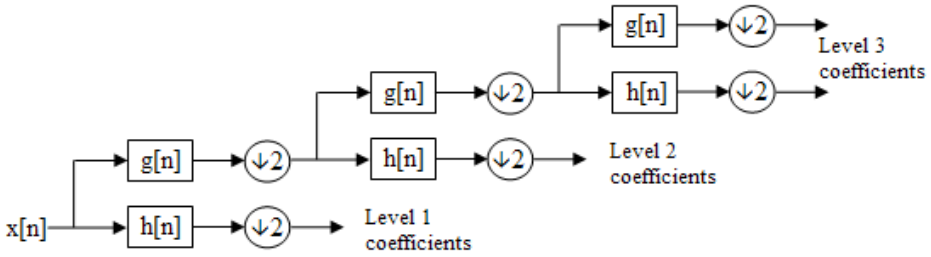

Figure 2.1: Three levels wavelet transform. x[n]: discrete signal of length n. g[n]:low pass filter. h[n]:high pass filter. ↓ 2:downsampling filter.

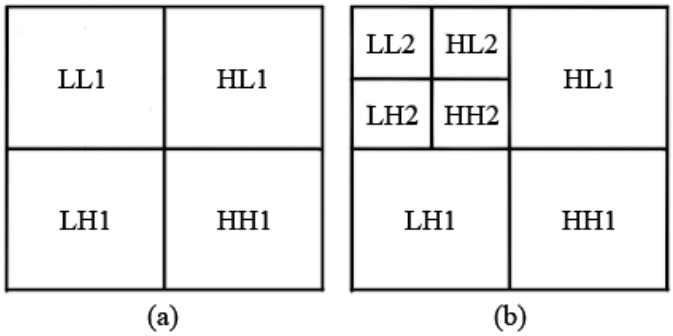

Figure 2.2: Wavelet transform. (a) and (b) are decimated wavelet decomposition diagrams, where the one-level and two-level case are shown, respectively.

in Fig.2.1. At each level in the above diagram the signal is decomposed into low-frequency and high-frequency.

The decomposition tiling of two-dimensional decimated wavelet transform is shown in Fig.2.2. After the decomposition, LL, LH, HL and HH components will be obtained. LL is the low frequency component of the image, and retains the primary information. LH and HL include horizontal and vertical edge information, respectively. HH contains diagonal information on the high frequency components. The detail information of image is represented in the HL, LH and HH subbands.

The wavelet transforms are relatively efficient for image restoration. However, its performance becomes worse for the regions which can generally be overcome by separable transforms (e.g., Haar and Symlets). Nevertheless, the representation of edges, textures, and gradual changing are inadequate with these separable transforms. To address this problem, the non-separable orthonormal transform was proposed to be applied to the image restoration so that its performance for textures and edges can be improved. However, this

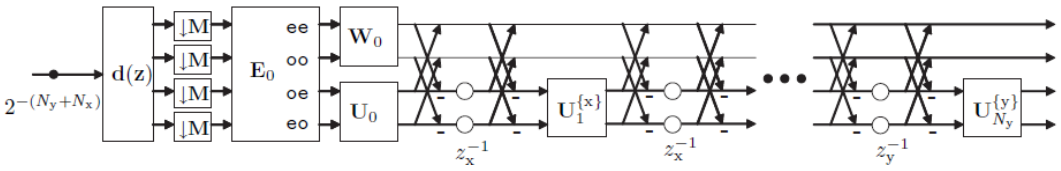

Figure 2.3: Lattice structure of a four channel analysis bank of DirLOT (forward transform), where $\mathbf{d}(\mathbf{z})$ is defined as a 2-D delay chain of size 4×1, M is the number of channels, symbols $\mathbf{W}_0$, $\mathbf{U}_0$ and $\mathbf{U}_{n_d}^{\{d\}}$ are orthonormal matrices with of size $M/2\times M/2$, $\mathbf{E}_0$ is an $M\times M$ symmetric orthonormal transform directly given by 2-D DCT, z_{x}^{-1} and z_{y}^{-1} are shifts of coefficients in the horizontal and vertical direction, respectively.

Table 2.1: Comparison of characteristics among transforms

Property	DirLOT	ISOWT	(5/3,9/7) DWT	Haar DWT	DCT
Orthogonality	Yes	Yes	No	Yes	Yes
Symmetry	Yes	Yes	Yes	Yes	Yes
Overlapping	Yes	Yes	Yes	No	No
Directivity	Yes	No	No	No	No

approach is only applicable to a fixed single geometric direction. In order to overcome the problem, a redundant transform with multiple DirLOTs was proposed so that the performance of image denoising can be improved [29].

2.3 Multiple Directional Transforms

In this section, we introduce a mixture of DirLOTs as a multi-directional transform [29], [30]. The multiple DirLOTs provide multi-scale decomposition and multi-directional decomposition. We use multiple DirLOTs to image restoration. It can take the features of images well and provide more information.

2.3.1 2-D Directional LOT

DirLOTs are able to completely satisfy the following three properties: orthogonality, symmetry, and overlapping property with a non-separable basis. This transform can be constructed with a lattice structure as shown in Fig.2.3. In addition, it can also satisfy the properties of fixed-critically-subsampling, real-valued, and compact-support. Furthermore, It can hold the trend vanishing moments (TVMs) for any direction. It is verified that the directional

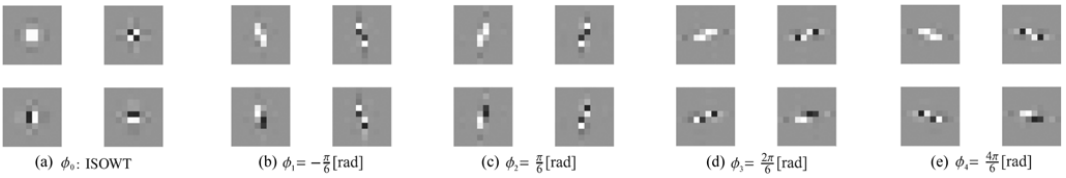

Figure 2.4: Examples of amplitude responses and bases of M-DirLOTs, where $[N_{\mathrm{y}}, N_{\mathrm{x}}]^T = [4, 4]^T$, i.e. the basis size is 10×10.

property works well for diagonal textures and edges. Table 2.1 shows comparison with other transforms.

The analysis polyphase matrix of order $[N_y, N_x]$ can be represented by

$$\mathbf{E}(\mathbf{z}) = \prod_{n_y=1}^{N_y} \{\mathbf{R}_{n_y}^{\{y\}} \mathbf{Q}(z_y)\} \cdot \prod_{n_x=1}^{N_x} \{\mathbf{R}_{n_x}^{\{x\}} \mathbf{Q}(z_x)\} \cdot \mathbf{R}_0 \mathbf{E}_0,$$

where

$$\mathbf{Q}(z_d) = \frac{1}{2} \begin{pmatrix} \mathbf{I}_{\frac{M}{2}} & \mathbf{I}_{\frac{M}{2}} \\ \mathbf{I}_{\frac{M}{2}} & -\mathbf{I}_{\frac{M}{2}} \end{pmatrix} \begin{pmatrix} \mathbf{I}_{\frac{M}{2}} & \mathbf{0}_{\frac{M}{2}} \\ \mathbf{0}_{\frac{M}{2}} & z_d^{-1} I_{\frac{M}{2}} \end{pmatrix} \begin{pmatrix} \mathbf{I}_{\frac{M}{2}} & \mathbf{I}_{\frac{M}{2}} \\ \mathbf{I}_{\frac{M}{2}} & -\mathbf{I}_{\frac{M}{2}} \end{pmatrix}$$

$$\mathbf{R}_0 = \begin{pmatrix} \mathbf{W}_0 & \mathbf{0}_{\frac{M}{2}} \\ \mathbf{0}_{\frac{M}{2}} & \mathbf{U}_0 \end{pmatrix}, \mathbf{R}_n^{\{d\}} = \begin{pmatrix} \mathbf{I}_{\frac{M}{2}} & \mathbf{0}_{\frac{M}{2}} \\ \mathbf{0}_{\frac{M}{2}} & \mathbf{U}_n^{\{d\}} \end{pmatrix},$$

$\mathbf{W}_0$, $\mathbf{U}_0$ and $\mathbf{U}_{n_d}^{\{d\}}$ are orthonormal matrices of size $M/2 \times M/2$. The M is the number of channels, i.e., $M = |\det \mathbf{M}|$. All of matrices $\mathbf{W}_0$, $\mathbf{U}_0$ and $\mathbf{U}_{n_d}^{\{d\}}$ can freely be controlled during the design process. $\mathbf{E}_0$ is an $M \times M$ symmetric orthonormal transform matrix given directly through the 2-D separable DCT. $\mathbf{I}$ is identity matrix of size $M/2 \times M/2$.

2.3.2 Multiple Directional LOTs

A single DirLOT is not suitable for images with oblique texture and edges in various directions. In order to express the geometric structures of image better, we define a dictionary $\mathbf{D}$ by M-DirLOTs as

$$\mathbf{D} = [\mathbf{\Psi}_{\phi_0}^T \ \mathbf{\Psi}_{\phi_1}^T \ \mathbf{\Psi}_{\phi_2}^T \ \mathbf{\Psi}_{\phi_3}^T \ ... \ \mathbf{\Psi}_{\phi_{R-1}}^T]^T,$$

where $\mathbf{\Psi}_{\phi_0}$ is a nondirectional isotropic symmetric orthonormal DWT (ISOWT) with the classical two-order vanishing moments (VMs) [31], and $\mathbf{\Psi}_{\phi_k}$ is a directional symmetric orthonormal wavelet transforms (DirSOWTs) constructed

by DirLOTs with the two-order TVMs for the direction ϕ_i. Fig.2.4 shows examples of atomic images in dictionary $\mathbf{D}$. R corresponds to the redundancy. The column vectors in $\mathbf{D}$ construct a normalized tight frame and satisfy

$$\mathbf{D}^T\mathbf{D} = \sum_{k=0}^{R-1} \mathbf{\Psi}_{\phi_k}^T \mathbf{\Psi}_{\phi_k} = R\mathbf{I},$$

which makes the image process simple.

2.3.3 Parameters Setting

In this thesis, some experimental results will be obtained with MATLAB R2014a implementation of our algorithm based on SaivDr Package. To promote the culture of reproducible research, the SaivDr Package can be accessed at http://www.mathworks.com/matlabcentral/fileexchange/45084-saivdr-package.

M-DirLOTs of polyphase order $[N_{\mathrm{y}}, N_{\mathrm{x}}]^T = [4, 4]^T$ were adopted. Since the basis size of DirLOTs is $L_{\mathrm{y}} \times L_{\mathrm{x}} = 10 \times 10$, Symlet of index 5, Sym5, was used as a reference of separable orthogonal DWT. The support size of the Symlet of index 5 is identical to the adopted DirLOTs. In order to achieve high-performance denoised image under relatively low redundancy. The TVM angles $\phi_1, \phi_2, \phi_3, \phi_4$ were set to $-\frac{\pi}{6}, \frac{\pi}{6}, \frac{2\pi}{6}$ and $\frac{4\pi}{6}$, respectively. Thus, the redundancy results in $R = 1 + 4 = 5$. The numbers of hierarchical level of M-DirLOTs were set to four.

3 Heuristic Poisson Denoising with M-DirLOTs

In this chapter, we detail the process of image denoising with M-DirLOTs. The heuristic shrinkage is applied.

3.1 Poisson Denoising based on VST

In this section, the Poisson noise , the SURE-LET, the Anscombe transform and its inverse transform are reviewed.

3.1.1 Poisson Noise

Suppose $\mathbf{x} = \{x_i\}$, $i = 0, ..., N-1$ is a noiseless image where N is the number of pixels. We use boldface $\mathbf{b}$ to denote the image observed through an image acquisition system. $\mathbf{b}$ consists of N independent Poisson random variables b_i depending on the underlying intensities x_i with $b_i \sim P(b_i|x_i)$. Each variable b_i can be considered as a Poisson random variable with the following probability density function

$$P(b_i|x_i) = e^{-x_i}\frac{x_i^{b_i}}{b_i!},$$

where x_i denotes the mean of b_i, which equals to its variance σ_i^2 for Poisson distribution. Therefore, the mean and the variance of the Poisson variable can be represented by

$$E\{b_i|x_i\} = \mathrm{Var}\{b_i|x_i\} = x_i.$$

Poisson noise $\mathbf{p} = \{p_i\}$ can be represented by

$$p_i = b_i - x_i = b_i - E\{b_i|x_i\}.$$

Thus, $E\{p_i|x_i\} = 0$ and $\mathrm{Var}\{p_i|x_i\} = x_i$.

Acquired $\mathbf{b}$ can be thought of as a noisy measurement of the intensity signal $\mathbf{x}$, where the noise is modeled as a Poisson noise.

3.1.2 Anscombe Transform

Because of the non-stability and the dependence on the underlying intensity of its variance, any existing Gaussian denoising algorithms cannot be directly applied to Poisson denoising model. Aiming at solving this problem, several VST methods have been adopted [4], [6], [9]. Among them, the Anscombe

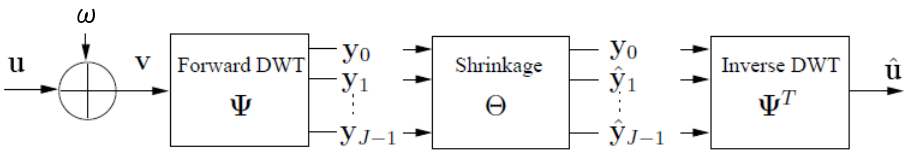

Figure 3.1: Principle of orthonormal wavelet denoising

transform was chosen because of its extensive application, efficiency, and simplicity [6]. The expression of the transform can be given by

$$v_i = f(b_i) = 2\sqrt{b_i + \frac{3}{8}},$$

where b_i and v_i denote the i-th pixel of the observed image contaminated by Poisson noise and the transformed data, respectively.

After performing the Anscombe transform, the noise throughout the whole image can be approximately modeled by Gaussian distributed. As a result, it is possible to apply Gaussian denoising algorithms. Inverse transform of the Anscombe transform is needed in order to return the variance-stabilized and denoised data to the original range. The Anscombe transform results in bias error, because it is a nonlinear forward transform. In order to minimize bias error, various inverse transforms were proposed. In this thesis, a closed-form approximation of this exact unbiased inverse

$$\hat{x}_i = \frac{1}{4}\hat{v}_i^2 + \frac{1}{4}\sqrt{\frac{3}{2}}\hat{v}_i^{-1} - \frac{11}{8}\hat{v}_i^{-2} + \frac{5}{8}\hat{v}_i^{-3} - \frac{1}{8}$$

is adopted [10].

3.1.3 SURE-LET Approach

The pixel values that were observed by an image acquisition device can be defined as $\mathbf{b} = (b_0, b_1, ...b_{N-1})^T$, where N is the number of pixels, and $(\cdot)^T$ is the transpose operator. $\mathbf{v} = (v_0, v_1, ..., v_{N-1})^T$ is the transformed data. The denoising problem of an image corrupted by Poisson noise is equivalent to restoring the noise-free image $\mathbf{u}$ from the transformed picture $\mathbf{v}$.

The picture $\mathbf{v}$ is considered to be corrupted with noise ω which is generally modeled as an additive white Gaussian noise (AWGN) with zero mean. Let $\mathbf{u}$ be the clean noiseless picture. Then, the transformed image $\mathbf{v}$ can be expressed by

$$\mathbf{v} = \mathbf{u} + \omega.$$

This image denoising problem becomes to find a good candidate $\hat{\mathbf{u}}$ of unknown noiseless picture $\mathbf{u}$ only from the transformed picture $\mathbf{v}$. Fig.3.1 shows the principle of orthonormal wavelet denoising, where Ψ, Θ and Ψ^T are the forward discrete wavelet transform (DWT), shrinkage function and inverse DWT, respectively. The quality of image denoising is determined by the transform Ψ and shrinkage function Θ.

The SURE-LET approach is a technique to realize the shrinkage function Θ. During the implementation of SURE-LET, all of a priori hypotheses are able to be avoided on the noiseless picture $\mathbf{u}$ under the AWGN assumption. Then, the denoising problem is reformulated as the search for the denoising process that minimizes the Stein's unbiased risk estimate (SURE). In [8], the point-wise thresholding

$$\theta(y) = \sum_{k=1}^{K} a_k y e^{-(k-1)\frac{y^2}{2T^2}},$$

was proposed, where y is a wavelet coefficient. In this function, $K = 2$ and $T = \sqrt{6}\sigma$ were suggested [8]. Moreover, the following form of the shrinkage function was proposed:

$$\theta(y, y_p; a, b) = e^{\frac{-y_p^2}{12\sigma^2}} \sum_{k=1}^{K} a_k y e^{-(k-1)\frac{y^2}{12\sigma^2}} + (1 - e^{\frac{-y_p^2}{12\sigma^2}}) \sum_{k=1}^{K} b_k y e^{-(k-1)\frac{y^2}{12\sigma^2}},$$

where y_p is an interscale prediction of y obtained from the wavelet parent-child relationship. The parameters a_k and b_k are linearly solved for minimizing SURE [32]. The parameters are determined by a solution of a system of linear equations for minimizing SURE for each transform and each image. This predictor tells us only an indication on its expected magnitude. Therefore, the parent y_p was used as a discriminator between high and low SNR wavelet coefficients.

In this section, a heuristic shrinkage is adopted. The heuristic shrinkage takes the average of the denoising results obtained by independent SURE-LET denoising with Ψ_{ϕ_k} for $k = 0, 1, \cdots, R-1$[33]. The heuristic shrinkage is available and simply realized by

$$\hat{\mathbf{u}} = \frac{1}{R}\mathbf{D}^T\Theta(\mathbf{D}\mathbf{v}) = \frac{1}{R}\sum_{k=0}^{R-1} \Psi_{\phi_k}^T \Theta(\Psi_{\phi_k}\mathbf{v}).$$

Note that SURE-LET is realized by a one-pass manner, where any of iteration, block-matching or direction/edge detection are not required, whereas the algorithm reaches the performance of the art in image denoising.

Figure 3.2: Poisson denoising results for "Lena". (a) Original image. (b) Noisy image (peak = 20): PSNR = 15.43 dB. (c), (d) and (e) are denoised results, through Sym5 (PSNR = 25.60 dB), ISOWT (PSNR = 25.68 dB) and multiple DirLOTs (PSNR = 26.23 dB), respectively.

Figure 3.3: Poisson denoising results for "Lena". (a) Noisy image (peak = 30): PSNR = 17.15 dB. (b), (c), (d) and (e) are denoised results, through TV (PSNR = 25.47 dB), ST-NLM (PSNR = 24.96 dB), PURE-LET (PSNR = 26.02 dB) and proposed method (PSNR = 26.94 dB), respectively.

3.2 Experimental Results

This section shows some experimental results of Poisson denoising in order to verify the significance of multiple DirLOTs based on VST. The combination of the SURE-LET approach as the shrinkage function and the M-DirLOTs as the DWT is evaluated. In addition, the interscale shrinkage function was adopted as in [8], where the parameter K was fixed to 2 and $T = \sqrt{6}\sigma$. The variance was estimated by applying the robust median estimator to the finest wavelet coefficients [34]. The results of Symlet of index 5 (Sym5), single ISOWT and DT-$\mathbb{C}$WT are also given as references.

3.2.1 Efficiencies of three transforms and four methods

Figs.3.2 and 3.3 show the first experimental results. In these experiments, "Lena" of size 128×128 pixels was used, where the noise level were set to peak = 20 and peak = 30, respectively. Peak intensity is varied by setting the maximum intensity of the noise-free signal. From Fig.3.2, it is observed that

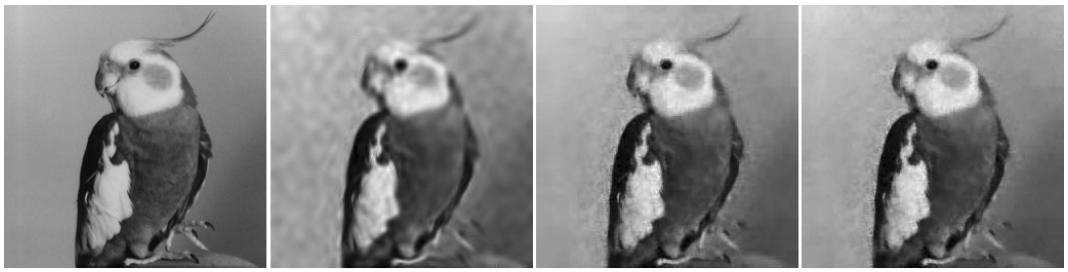

(a) (b) (c) (d)

Figure 3.4: Poisson denoising results when peak = 30 for "Coco". (a) Original image. (b), (c) and (d) are denoised results, through DT-ℂWT, multiple DirLOTs (BiShrink) and proposed method, respectively.

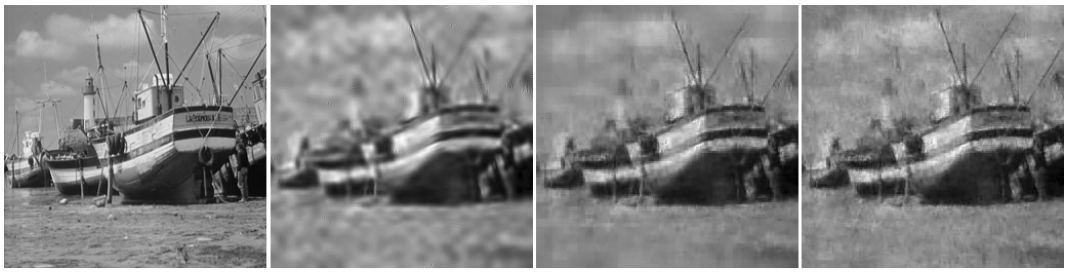

(a) (b) (c) (d)

Figure 3.5: Poisson denoising results when peak = 10 for "Boat". (a) Original image. (b), (c) and (d) are denoised results, through DT-ℂWT, multiple DirLOTs (BiShrink) and proposed method, respectively.

multiple DirLOTs shows better performance for diagonal edges and gradual changing (e.g., edge of hat and face) among four transforms. In Fig.3.3, we can also see that the multiple DirLOTs shows better quality for edges and detail informations (e.g., edge of hat, eye and plush) compared with the other three methods.

3.2.2 Performances of DT-ℂWT and M-DirLOTs

In the second experiment, eight images "Coco", "Boat", "Baboon", "Man", "Cameraman", "Saturn", "Peppers" and "Opthalmic", were used, where the sizes are all 256×256 pixels. "Cameraman" adopted here is a part of original Cameraman of size 512×512. Peak signal-to-noise ratio (PSNR) and normalized mean integrated squared error (NMISE) were used as performance metrics for evaluating image restoration problem. The NMISE takes the noise variance

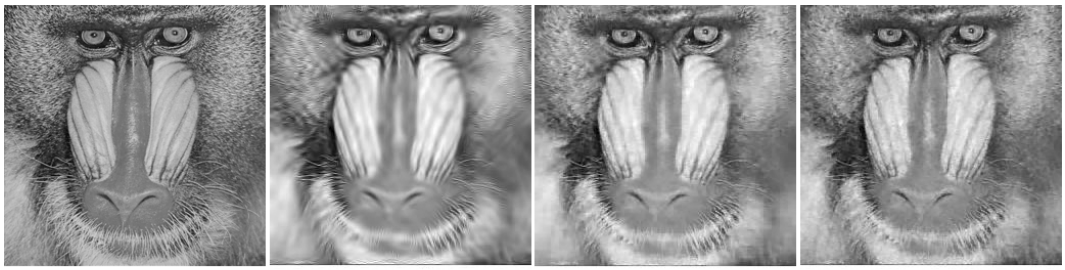

(a) (b) (c) (d)

Figure 3.6: Poisson denoising results when peak = 60 for "Baboon". (a) Original image. (b), (c) and (d) are denoised results, through DT-ℂWT, multiple DirLOTs (BiShrink) and proposed method, respectively.

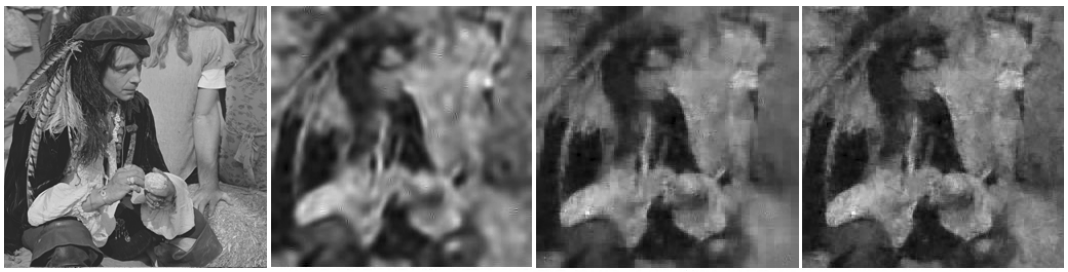

(a) (b) (c) (d)

Figure 3.7: Poisson denoising results when peak = 5 for "Man". (a) Original image. (b), (c) and (d) are denoised results, through DT-ℂWT, multiple DirLOTs (BiShrink) and proposed method, respectively.

of the Poisson process into account. In order to shrink the complex-valued coefficients of DT-ℂWT, locally adaptive Bivariate Shrinkage (BiShrink, [7×7]) was used [35].

Figs.3.4-3.7 show parts of the experimental results based on VST-BiShrink and proposed method. Figs.3.8-3.11 show parts of the experimental results based on VST and SURE-LET. It can be seen that the quality of denoising image with the multiple DirLOTs is better than the results of Sym5, ISOWT and DT-ℂWT. Figs.3.4-3.7 show that image denoising can be improved for diagonal edges by multiple DirLOTs. Observing Fig.3.8, we see better quality result for diagonal textures than the results of Sym5 and ISOWT. Fig.3.9 shows better performance for gradual changing and edges (e.g., central part). Figs.3.10-3.11 show better denoising performance for gradual changing.

By contrast, it can be seen that the noise has been effectively reduced for diagonal textures, edges and gradation. The multiple DirLOTs improved the

Table 3.1: Comparison of PSNRs and NMISEs between two transforms among three methods. BiShrink and Proposed denoted as B and P, respectively.

Peak	PSNR [dB]						NMISE					
	5	10	20	30	60	120	5	10	20	30	60	120
Image	Coco											
DT-ℂWT(B)	24.73	26.49	28.68	29.70	31.73	33.74	**0.04**	**0.05**	**0.06**	0.08	**0.09**	0.12
M-DirLOTs(B)	25.57	27.19	29.12	30.18	31.89	33.73	**0.04**	**0.05**	**0.06**	**0.07**	**0.09**	**0.11**
M-DirLOTs(P)	**25.63**	**27.21**	**29.22**	**30.28**	**31.96**	**33.80**	**0.04**	**0.05**	**0.06**	**0.07**	**0.09**	**0.11**
Image	Boat											
DT-ℂWT(B)	21.93	23.03	24.57	25.47	27.18	28.85	0.08	0.12	0.17	0.20	0.26	0.34
M-DirLOTs(B)	22.44	23.54	25.22	26.12	27.67	**29.47**	0.08	**0.11**	**0.14**	**0.17**	**0.23**	**0.30**
M-DirLOTs(P)	**22.55**	**23.66**	**25.33**	**26.22**	**27.73**	29.45	**0.07**	**0.11**	**0.14**	**0.17**	**0.23**	**0.30**
Image	Baboon											
DT-ℂWT(B)	19.99	20.58	21.39	21.98	23.41	25.01	0.10	0.18	0.29	0.37	0.52	0.70
M-DirLOTs(B)	20.17	20.85	21.77	22.43	23.93	25.42	0.10	0.17	0.26	0.34	0.46	0.64
M-DirLOTs(P)	**20.46**	**21.28**	**22.21**	**22.89**	**24.26**	**25.52**	**0.09**	**0.15**	**0.24**	**0.30**	**0.42**	**0.62**
Image	Man											
DT-ℂWT(B)	21.79	23.03	24.24	25.13	26.63	28.42	0.08	0.12	0.17	0.21	0.29	0.38
M-DirLOTs(B)	22.07	23.44	24.82	25.83	27.45	29.19	**0.07**	0.11	0.15	0.18	0.24	0.32
M-DirLOTs(P)	**22.36**	**23.68**	**25.09**	**25.98**	**27.58**	**29.26**	**0.07**	**0.10**	**0.14**	**0.17**	**0.23**	**0.31**

denoising performance for natural images which contain rich amount of geometrical structures. In Table 3.1, the multiple DirLOTs shows better quality compared with the results of DT-ℂWT. Simultaneously, the proposed method shows better results than the BiShrink ([7×7]) with multiple DirLOTs. The denoising performances among three transforms for various noise levels are compared in Table 3.2. In Table 3.2, we see that the proposed multiple DirLOTs achieve the highest PSNRs and the smallest NMISEs for all the peak values in the four images. The union of multiple DirLOTs shows the best performance among the three transforms in the second experiment.

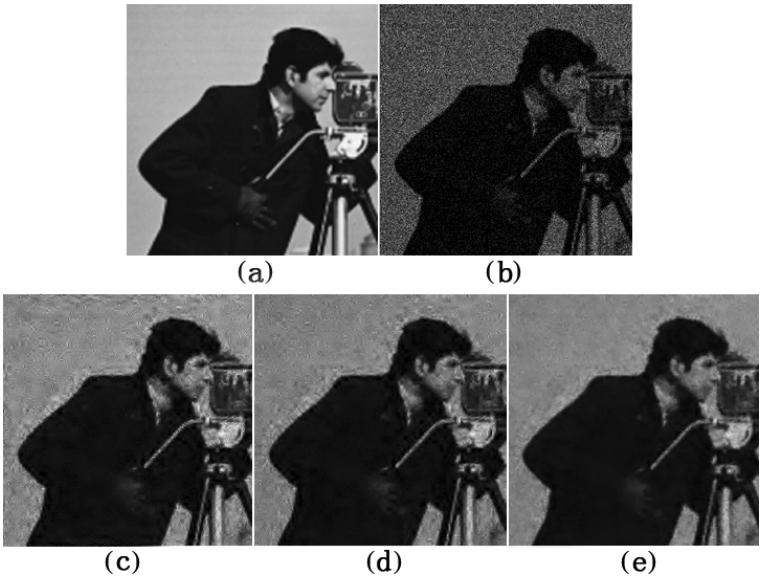

Figure 3.8: Poisson denoising results for "Cameraman". (a) Original image. (b) Noisy image (peak = 10). (c), (d) and (e) are denoised results, through Sym5, ISOWT and multiple DirLOTs, respectively.

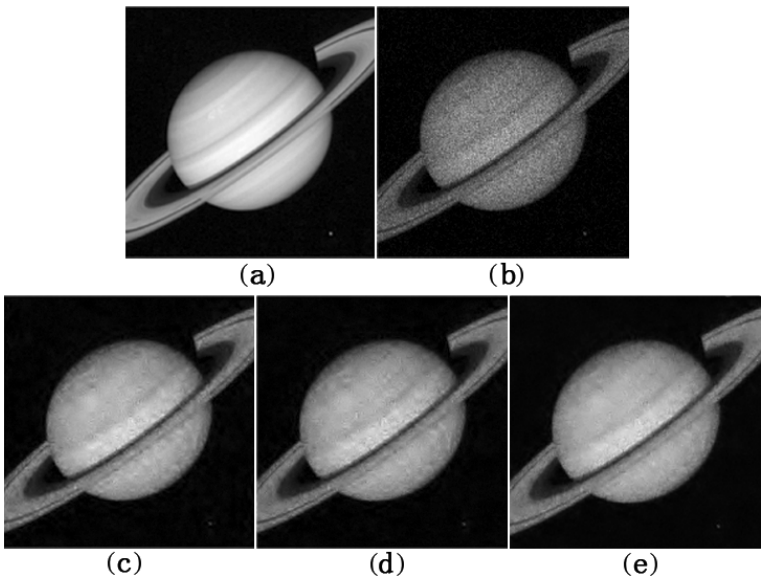

Figure 3.9: Poisson denoising results for "Saturn". (a) Original image. (b) Noisy image (peak = 30). (c), (d) and (e) are denoised results, through Sym5, ISOWT and multiple DirLOTs, respectively.

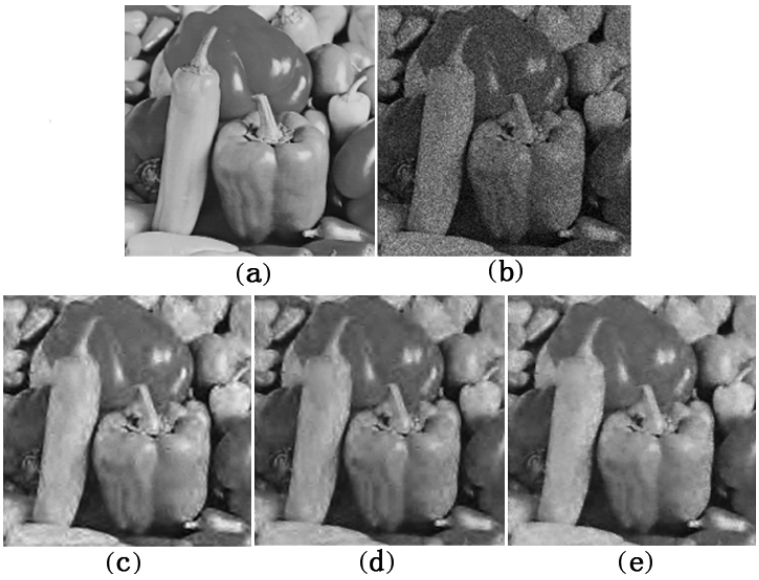

Figure 3.10: Poisson denoising results for "Peppers". (a) Original image. (b) Noisy image (peak = 20). (c), (d) and (e) are denoised results, through Sym5, ISOWT and multiple DirLOTs, respectively.

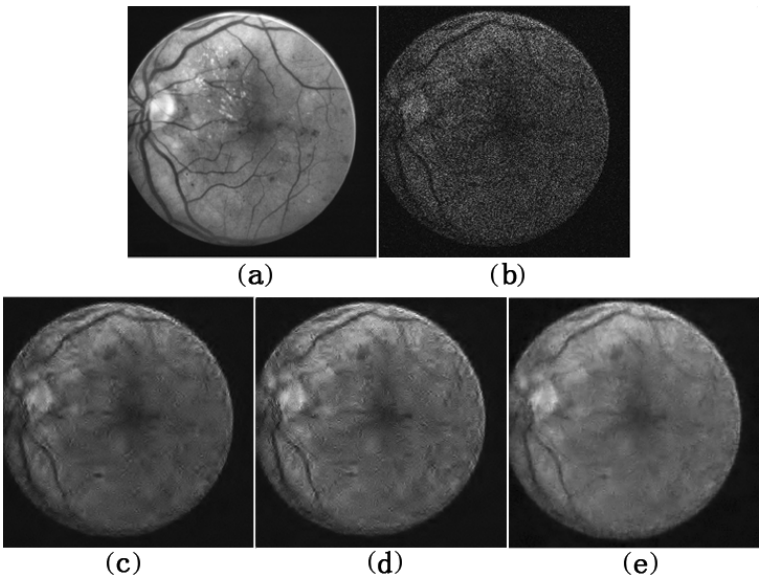

Figure 3.11: Poisson denoising results for "Opthalmic". (a) Original image. (b) Noisy image (peak = 10). (c), (d) and (e) are denoised results, through Sym5, ISOWT and multiple DirLOTs, respectively.

Table 3.2: Comparison of PSNRs and NMISEs among three transforms based on VST and SURE-LET

Image	Peak	Noise	PSNR [dB]			NMISE		
			Sym5	ISOWT	M-DirLOTs	Sym5	ISOWT	M-DirLOTs
Camera-man	5	11.44	18.03	18.38	**19.90**	0.21	0.19	**0.14**
	10	14.48	24.29	24.35	**25.34**	0.12	0.11	**0.09**
	20	17.48	27.96	28.14	**28.79**	0.11	0.11	**0.09**
	30	19.21	29.36	29.49	**30.22**	0.12	0.12	**0.10**
	60	22.23	31.38	31.43	**32.32**	0.15	0.15	**0.12**
	120	25.23	33.53	33.66	**34.31**	0.18	0.18	**0.15**
Saturn	5	12.67	**14.12**	13.75	**14.12**	0.41	0.41	**0.36**
	10	15.48	19.16	19.49	**20.70**	0.30	0.29	**0.22**
	20	18.57	25.71	25.92	**26.69**	0.19	0.19	**0.15**
	30	20.26	29.07	29.24	**30.18**	0.15	0.14	**0.12**
	60	23.36	33.50	33.53	**34.03**	0.15	0.14	**0.13**
	120	26.32	35.34	35.38	**35.94**	0.21	0.21	**0.19**
Peppers	5	10.12	22.16	22.06	**22.53**	0.07	0.08	**0.07**
	10	13.18	23.95	23.85	**24.38**	0.10	0.10	**0.09**
	20	16.15	25.94	25.92	**26.53**	0.12	0.13	**0.11**
	30	17.92	26.85	26.80	**27.46**	0.15	0.15	**0.13**
	60	20.93	28.67	28.61	**29.22**	0.19	0.20	**0.17**
	120	23.94	30.53	30.46	**30.96**	0.24	0.25	**0.23**
Opthalmic	5	11.79	20.28	20.65	**22.06**	0.14	0.12	**0.09**
	10	14.71	24.97	25.08	**26.24**	0.09	0.08	**0.06**
	20	17.73	28.77	28.71	**28.96**	**0.07**	**0.07**	**0.07**
	30	19.50	29.59	29.52	**29.86**	0.09	0.09	**0.08**
	60	22.49	31.35	31.31	**31.50**	0.12	0.12	**0.12**
	120	25.52	32.85	32.80	**33.03**	0.17	0.17	**0.16**

Table 3.3: Comparison of average computation times for Lena (256×256) and Cameraman (512×512)

Image	TV	ST-NLM	PURE-LET	Proposed
Lena	43.45 s	69.50 s	0.37 s	0.96 s
Cameraman	280.61 s	349.04 s	1.52 s	3.04 s

3.2.3 Comparison with State-of-the-art Methods

In the third experiment, "House", "Brain", "Barbara" and "Lena", were used, where the sizes are all 256×256 pixels. The TV, ST-NLM, PURE-LET algorithm were used as references, where three algorithms were implemented using MATLAB programs provided by their authors [36], [37], [38]. The TV method is the usual total variation regularization [39]. The ST-NLM (stabilized version of NL means) method adopted the Non-Local means (NL means) filter based on VST [40], [41]. The redundancy of adopted transform in PURE-LET was set to five [2].

Figs.3.12-3.15 show the experimental results among four method for various peak intensities. It can be seen that the quality for detail informations, diagonal textures and edges (e.g., housetop) of denoising image with the multiple DirLOTs is better than the results of the other methods in Fig.3.12. In Fig.3.13, we can see that the proposed method shows better quality for edges, detail informations and gradual changing. Figs.3.14-3.15 show better denoising performance for detail informations and edges. For PSNRs in Table 3.4, we can see that the proposed method achieve the highest PSNR for all the four images. It can be seen from Table 3.4 that the proposed method achieve smallest NMISEs for all the peak values in the four images among the four method. We also compared computation times among the four methods in Table 3.3. The computation times have been averaged over 10 noise realizations. In the case of Lena of size 256×256, the computation time of the proposed method is about 2.2% and 1.4% of TV and ST-NLM, respectively. In the case of Cameraman of size 512×512, it is about 1.1% and 0.9%. For these two cases, computation times are the same order of that of the PURE-LET.

The experimental results imply that the multiple DirLOTs are not only able to reproduce the diagonal structure appropriately, but also generate fairly good results. By introducing directional decomposition into the transform, can efficiently obtain diagonal components present in natural images.

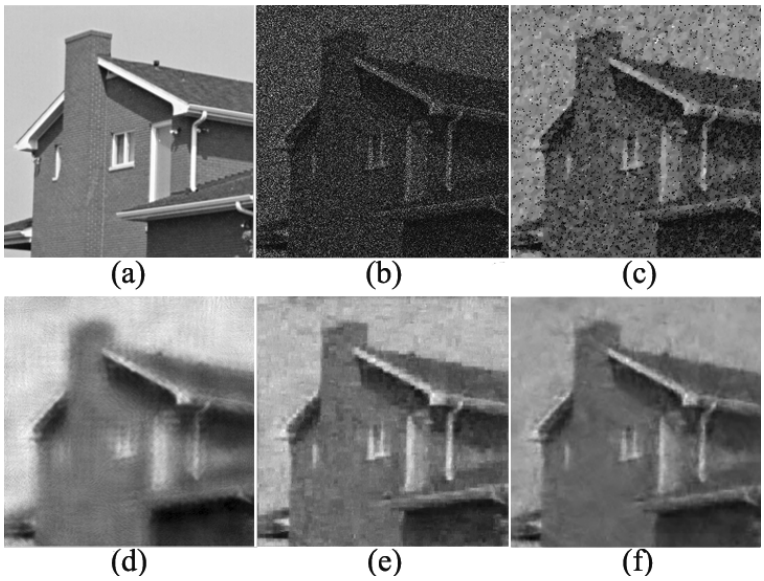

Figure 3.12: Poisson denoising results for "House". (a) Original image. (b) Noisy image (peak = 5). (c), (d), (e) and (f) are denoised results, through TV, ST-NLM, PURE-LET and proposed method, respectively.

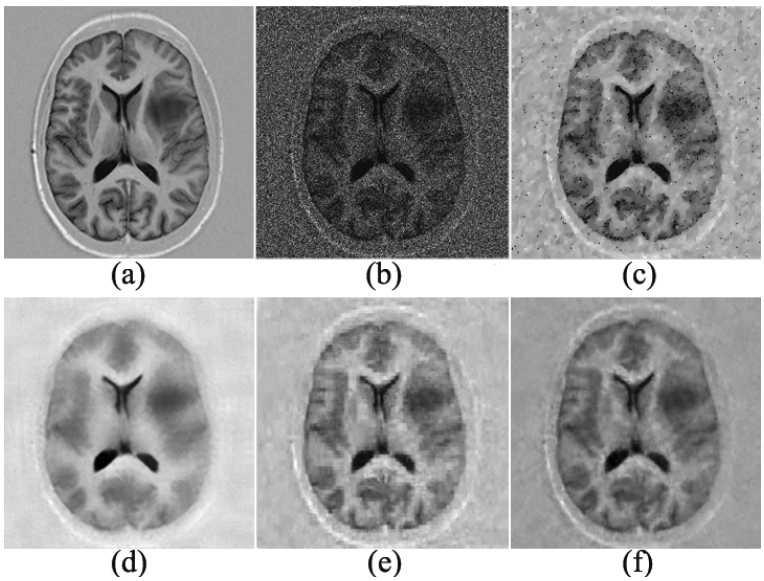

Figure 3.13: Poisson denoising results for "Brain". (a) Original image. (b) Noisy image (peak = 10). (c), (d), (e) and (f) are denoised results, through TV, ST-NLM, PURE-LET and proposed method, respectively.

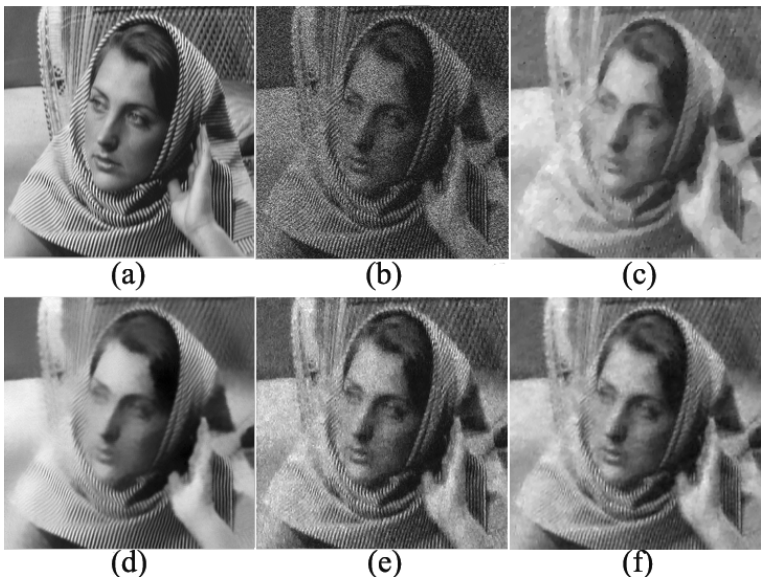

Figure 3.14: Poisson denoising results for "Barbara". (a) Original image. (b) Noisy image (peak = 30). (c), (d), (e) and (f) are denoised results, through TV, ST-NLM, PURE-LET and proposed method, respectively.

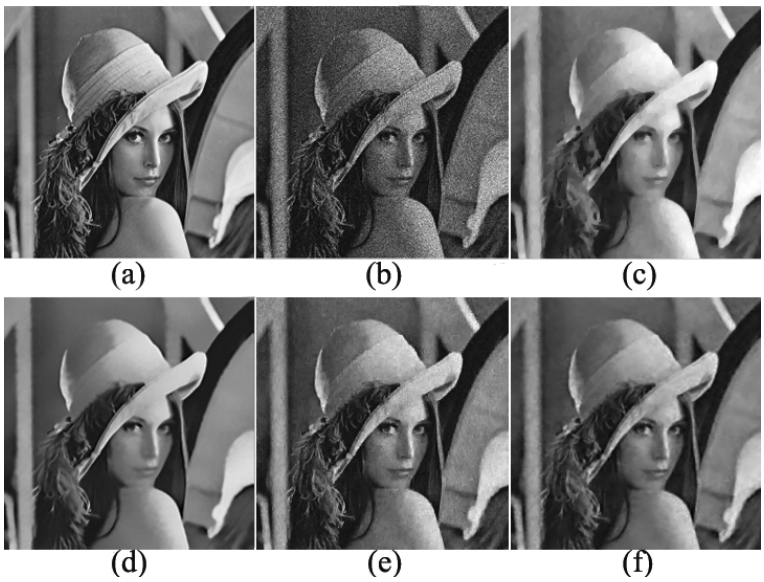

Figure 3.15: Poisson denoising results for "Lena". (a) Original image. (b) Noisy image (peak = 60). (c), (d), (e) and (f) are denoised results, through TV, ST-NLM, PURE-LET and proposed method, respectively.

Table 3.4: Comparison of PSNRs and NMISEs among four methods for various peak intensities

Peak	PSNR [dB]						NMISE					
	5	10	20	30	60	120	5	10	20	30	60	120
Image	House											
TV	15.78	22.83	26.24	26.77	27.74	12.91	0.26	0.11	0.09	0.11	0.18	10.74
ST-NLM	20.28	22.77	24.96	26.09	28.85	31.61	0.07	0.09	0.11	0.13	0.15	0.17
PURE-LET	23.92	25.43	27.12	27.79	29.72	31.55	0.04	0.06	0.08	0.10	0.13	0.16
Proposed	**24.41**	**25.95**	**27.57**	**28.45**	**30.31**	**31.92**	**0.03**	**0.05**	**0.07**	**0.08**	**0.11**	**0.15**
Image	Brain											
TV	15.66	23.04	26.64	27.23	27.83	28.18	0.27	0.11	0.10	0.14	0.26	0.49
ST-NLM	21.30	23.60	25.23	26.12	27.95	30.17	0.10	0.12	0.15	0.18	0.22	0.25
PURE-LET	23.99	25.56	27.17	27.99	29.72	31.53	0.08	0.10	0.12	0.14	0.17	0.20
Proposed	**24.67**	**26.04**	**27.73**	**28.58**	**30.49**	**32.23**	**0.06**	**0.07**	**0.08**	**0.10**	**0.12**	**0.16**
Image	Barbara											
TV	15.24	19.86	21.41	21.56	21.72	14.21	0.33	0.25	0.34	0.49	0.96	8.29
ST-NLM	18.79	20.31	21.97	23.02	25.32	27.97	0.13	0.19	0.27	0.32	0.38	0.41
PURE-LET	20.74	21.79	23.00	24.06	25.69	27.85	**0.10**	0.16	0.23	0.27	0.35	**0.41**
Proposed	**20.82**	**22.01**	**23.28**	**24.19**	**26.09**	**27.99**	**0.10**	**0.14**	**0.21**	**0.26**	**0.32**	**0.41**
Image	Lena											
TV [39]	16.12	21.46	24.65	25.27	25.91	26.21	0.34	0.24	0.23	0.29	0.51	1.01
ST-NLM [41]	19.45	22.04	24.36	25.64	27.98	30.46	0.15	0.18	0.23	0.26	0.32	0.35
PURE-LET [2]	22.96	24.18	25.64	26.57	28.55	30.36	0.11	0.15	0.21	0.24	0.28	0.35
Proposed	**23.00**	**24.48**	**26.24**	**27.26**	**29.08**	**30.88**	**0.09**	**0.12**	**0.16**	**0.18**	**0.24**	**0.31**

3.3 Summary

The SURE-LET approach for Poisson denoising was reviewed as an orthonormal wavelet-based denoising technique. There was a disadvantage that the representation of diagonal geometric structures is relatively insufficient by using traditional separable transform. Therefore, we proposed to adopt the multiple DirLOTs in order to improve the SURE-LET approach and applied it to removing Poisson noise by introducing VST. Experimental results show that the combination of the VST, SURE-LET, and multiple DirLOTs significantly improved the denoising performance, and their effectiveness has been verified.

4 Heuristic Image Fusion with M-DirLOTs

In this section, let us review an image fusion technique based on DWT, and specify the fusion rule.

4.1 Fusion framework based on DWT

The decomposition tiling of two-dimensional wavelet transform is shown in Fig.2.2. After the decomposition, LL, LH, HL and HH components will be obtained. LL is the low frequency component of the image, and retains the primary information. LH and HL include horizontal and vertical edge information, respectively. HH contains diagonal information on the high frequency components. The detail information of image is represented in the HL, LH and HH subbands.

A framework of an image fusion system based on one-level DWT is illustrated in Fig.1.2. Although fusion of two images is illustrated, the fusion of multiple images can also be achieved by analogy. In Fig.1.2, A and B are two original images, and F is a fused image. The basic steps of the procedure are as follows:

1. DWT decomposition is applied to every image to analyze the subband coefficients. LL_ℓ, LH_ℓ, HL_ℓ and HH_ℓ are approximation information, horizontal edge information, vertical edge information and diagonal information, respectively, where ℓ denotes the decomposition level.
2. Each subband is fused independently. Different fusion algorithms can be used to process individual subband.
3. The inverse DWT is applied to generate a fused image.

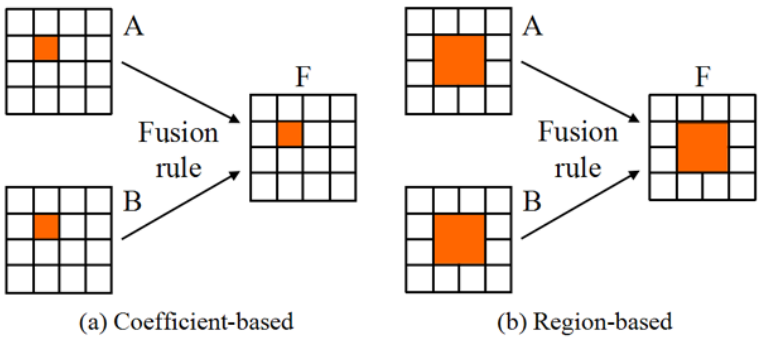

Figure 4.1: Coefficient-based and region-based approaches.

In detail, there are two types of fusion rules for fusing the subbands; the coefficient-based and region-based approaches. In Fig.4.1, the coefficient-based and region-based approaches are shown. In the coefficient-based fusion, the wavelet coefficients are fused by selecting the either value on corresponding position or taking weighted coefficient of two coefficients. For the region-based fusion, the wavelet coefficients in local windows are fused. A new pixel value will be a center value of window A if fusing parameters of window A is greater than one of the corresponding window B. In this thesis, the coefficient-based approach is discussed.

Considering characteristics of wavelet coefficients, an image fusion rule (denoted as Θ) and forward DWT (denoted as $\mathbf{\Psi}$) are chosen. The above fusion algorithm is compactly expressed by

$$\mathbf{x}_F = \mathbf{\Psi}^{-1}\mathbf{c}_F = \mathbf{\Psi}^{-1}\Theta(\mathbf{\Psi}\mathbf{x}_A, \mathbf{\Psi}\mathbf{x}_B),$$

where $\mathbf{x}_A$, $\mathbf{x}_B$ and $\mathbf{x}_F$ are vector representations of input image A, input image B and fused image F, respectively. $\mathbf{c}_F$ is the vector representation of the fused coefficients. The fusion rule Θ usually takes the average value, standard deviation, energy, etc.

4.1.1 Combination of Approximation Subband

Let $\mathbf{c}_A^L$ and $\mathbf{c}_B^L$ be approximation wavelet coefficients of $\mathbf{\Psi}\mathbf{x}_A$ and $\mathbf{\Psi}\mathbf{x}_B$, respectively, and $\mathbf{c}_F^L$ is an approximation coefficient of $\mathbf{c}_F$. A classical fusion rule uses average values for low-frequency coefficients [43]. The relationship among the approximation coefficients is represented by

$$\mathbf{c}_F^L = \Theta^L(\mathbf{c}_A, \mathbf{c}_B) = \frac{1}{2}(\mathbf{c}_A^L + \mathbf{c}_B^L).$$

4.1.2 Combination of Detail Subbands

Image information about salient features of a given picture, such as edges appears as wavelet coefficients of large absolute values. Thus, it is convenient to extract suitable absolute values of the corresponding wavelet coefficients. Many distinctive focus measurements measure the variation of coefficients. Coefficients with properer values of these measurements, when multiple original images are compared, are considered from clear parts and selected as the coefficients of the fused image. Compared among many measurements, the sum-modified-Laplacian (SML) is a good measurement for detail subbands[44]. Let $\mathbf{c}_A^H$, $\mathbf{c}_B^H$ and $\mathbf{c}_F^H$ be the detail wavelet coefficients (i.e. LH_ℓ, HL_ℓ and HH_ℓ)

of $\mathbf{\Psi x}_A$, $\mathbf{\Psi x}_B$ and $\mathbf{c}_F$, respectively. The SML is defined as follows:

$$\mathrm{SML}^{H,\ell,k}(i,j) = \sum_{r=-W}^{W} \sum_{c=-L}^{L} [\mathrm{ML}^{H,\ell,k}(i+r, j+c)],$$

where $\mathrm{ML}^{H,\ell,k}$ is modified Laplacian. The parameters W and L set the window size $(2W+1) \times (2L+1)$, which are used to compute the $\mathrm{SML}^{H,\ell,k}$. If we set the size of the window to 3×3, then the $\mathrm{ML}^{H,\ell,k}$ is defined by

$$\begin{aligned}\mathrm{ML}^{H,\ell,k}(i,j) = &|2\mathbf{c}^{H,\ell,k}(i,j) - \mathbf{c}^{H,\ell,k}(i-\delta,j) - \mathbf{c}^{H,\ell,k}(i+\delta,j)| \\ &+|2\mathbf{c}^{H,\ell,k}(i,j) - \mathbf{c}^{H,\ell,k}(i,j-\delta) - \mathbf{c}^{H,\ell,k}(i,j+\delta)|,\end{aligned}$$

where $\mathbf{c}^{H,\ell,k}(i,j)$ denotes the coefficient located at (i,j) in the ℓ-th decomposition level and k-th subband. Symbol δ is a spacing variable between coefficients to compute ML and often set to 1.

Considering the human visual contrast (e.g., sensitivity to local contrast change, edges, and directional features), the local luminance contrast was developed [45]. SML based on visual contrast (VC) is given by

$$\mathrm{VC}_{\mathrm{SML}}^{H,\ell,k}(i,j) = \begin{cases} \dfrac{\mathrm{SML}^{H,\ell,k}(i,j)}{(\bar{\mathbf{c}}^{L,\ell}(i,j))^{1+\alpha}}, & \text{if } \bar{\mathbf{c}}^{L,\ell}(i,j) \neq 0 \\ \mathrm{SML}^{H,\ell,k}(i,j), & \text{otherwise} \end{cases}, \tag{1}$$

where $\bar{\mathbf{c}}^{L,\ell}(i,j)$ is the mean coefficient of approximation subband of the corresponding detail subband at the position (i,j) centered of the window for the same scale. α is a visual constant, which is set by perceptual experiment, ranging from 0.6 to 0.7 [46].

The detail subband of the fused image denoted as $\mathbf{c}_F^{H,\ell,k}(i,j)$ is given by

$$\begin{aligned}\mathbf{c}_F^{H,\ell,k}(i,j) &= \Theta^{H,\ell,k}(\mathbf{c}_A, \mathbf{c}_B) \\ &= \begin{cases} \mathbf{c}_A^{H,\ell,k}(i,j), \text{ if } \mathrm{VC}_{\mathrm{SML}}^{H_A,\ell,k}(i,j) \geq \mathrm{VC}_{\mathrm{SML}}^{H_B,\ell,k}(i,j) \\ \mathbf{c}_B^{H,\ell,k}(i,j), \text{ otherwise} \end{cases},\end{aligned}$$

where $\mathrm{VC}_{\mathrm{SML}}^{H_A,\ell,k}(i,j)$ and $\mathrm{VC}_{\mathrm{SML}}^{H_B,\ell,k}(i,j)$ are $\mathrm{VC}_{\mathrm{SML}}^{H,\ell,k}$ of detail subbands of the corresponding image A and B at location (i,j), respectively.

4.1.3 Focused Region Detection

In [21], an identification method of the focused region based on classical fusion rule was introduced. The detection of focused regions can be presented

as following steps:

1. Apply DWT to source images (A and B). The lowpass subband and the highpass subbands coefficients are fused. The inverse DWT is applied to get an initial fused image.
2. Calculate the RMSE (root mean square error) of each pixel within a local area between the source images and the initial fused image.
3. Compare the value $\mathrm{RMSE}_A(i,j)$ and $\mathrm{RMSE}_B(i,j)$ to determine logical matrix $\mathbf{Z}$ (binary image), where '1' in $\mathbf{Z}$ indicates the pixel at position (i,j) in image A is fused ($\mathrm{RMSE}_A(i,j) \leq \mathrm{RMSE}_B(i,j)$) and '0' indicates the pixel in B is fused.
4. Morphological opening ($\mathbf{Z} \circ \mathbf{B}$) and closing ($\mathbf{Z} \bullet \mathbf{B}$) with small structural element are used to optimize $\mathbf{Z}$ (thin connections, thin protrusions, narrow breaks, fill long thin gulfs). Meanwhile, a threshold T_{th} is set to remove the holes smaller than the threshold. The structural element $\mathbf{B}$ is a 4×4 matrix with logical 1's and T_{th} is set according to the experimental results. The resulting logical matrix denoted as $\mathbf{Z}'$. Morphological operations are again performed to smooth object contours [47].
5. The final image F is constructed by the map $\mathbf{Z}'$.

4.1.4 Proposed Fusion Rule

In [45], the local luminance contrast can be understood as contrast of high-frequency component and low-frequency component in wavelet domain. It is defined as

$$C = \frac{L' - L_B}{L_B} = \frac{\triangle L}{L_B},$$

where L' and L_B are local gray level and local brightness of the background, respectively. L_B and $\triangle L$ correspond to low-frequency component and high-frequency component, respectively. The traditional contrast measurement (e.g., $\mathrm{VC}_{\mathrm{SML}}$) was based on this feature. In Eq.(1), the low-frequency components at the same scale were used to calculate $\mathrm{VC}_{\mathrm{SML}}$ of detail subbands. However, the performance is weak since low-pass subband at the same scale contains some high-frequency components.

In order to improve the characteristics of VC, we suggest to adopt piecewise constant low-frequency information. We propose to build an interscale predictor of the same size as LL_ℓ from the deepest low-pass scale through

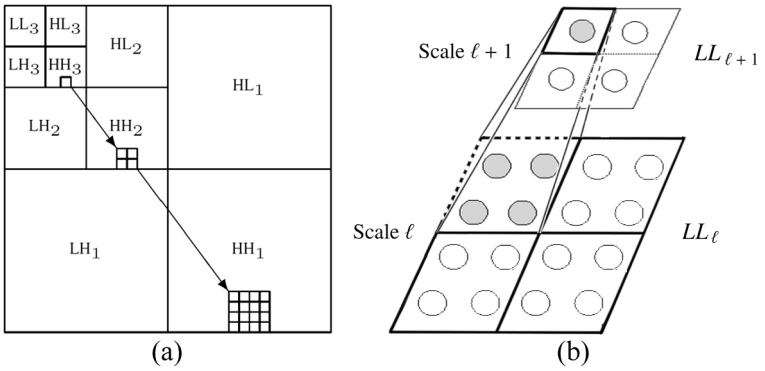

Figure 4.2: (a) Subband tile of maximally decimated orthogonal wavelet transform. (b) Example of interscale relation.

nearest neighbor interpolation. We define interscale VC ($\mathrm{IVC_{SML}}$) as

$$\mathrm{IVC}_{\mathrm{SML}}^{H,\ell,k}(i,j) = \begin{cases} \dfrac{\mathrm{SML}^{H,\ell,k}(i,j)}{(\bar{\mathbf{c}}_p^{L,\ell}(i,j))^{1+\alpha}}, & \text{if } \bar{\mathbf{c}}_p^{L,\ell}(i,j) \neq 0 \\ \mathrm{SML}^{H,\ell,k}(i,j), & \text{otherwise} \end{cases},$$

where $\bar{\mathbf{c}}_p^{L,\ell}$ is the mean coefficient of predictor coefficient at the position (i,j) centered of the window for the same scale. α is a visual constant ranging from 0.6 to 0.7. $\mathrm{SML}^{H,\ell,k}$ denotes SML in the ℓ-th decomposition level and k-th high-frequency subband. Fig.4.2 show the subband tile of maximally decimated orthogonal wavelet transform and the interscale relation between low-frequency subband and interscale predictor.

For the purpose of better performance, the highpass subbands coefficients are merged by the IVC maximum choosing scheme discussed in Section 4.1.2. The fused detail coefficients denoted as $\mathbf{c}_F^{H,\ell,k}(i,j)$ is given by

$$\begin{aligned} \mathbf{c}_F^{H,\ell,k}(i,j) &= \Theta^{H,\ell,k}(\mathbf{c}_A, \mathbf{c}_B) \\ &= \begin{cases} \mathbf{c}_A^{H,\ell,k}(i,j), \text{ if } \mathrm{IVC}_{\mathrm{SML}}^{H_A,\ell,k}(i,j) \geq \mathrm{IVC}_{\mathrm{SML}}^{H_B,\ell,k}(i,j) \\ \mathbf{c}_B^{H,\ell,k}(i,j), \text{ otherwise} \end{cases}. \end{aligned}$$

After focused regions detection, the fused image is obtained. Unfortunately, the fused image may contain many erroneous results at the edge of the focused regions. In addition, our proposed method selects the fusion pixels of the focused border regions from the $\mathbf{Z}$. Therefore, we construct the final map $\mathbf{Z}'$

Table 4.1: Adopted transforms and the features

Abrv.	Features	R
UDHT	Undecimated Haar wavelet decomposition level is set to two	7
NSCT	Nonsubsampled contourlet $[2^2, 2^3, 2^3, 2^4]$ directions	36
NSST	Nonsubsampled shearlet $[2^3, 2^3, 2^4, 2^4]$ directions	49
M-DirLOTs	Polyphase order $[N_{\mathrm{y}}, N_{\mathrm{x}}]^T = [4, 4]^T$ Classical VM+TVM w directions $[-\frac{\pi}{6}, \frac{\pi}{6}, \frac{2\pi}{6}, \frac{4\pi}{6}]$	5

as

$$\mathbf{Z}'(i,j) = \begin{cases} 1, & \text{if} \quad \mathbf{s}(i,j) = mn \\ 0, & \text{if} \quad \mathbf{s}(i,j) = 0 \\ \mathbf{Z}(i,j), & \text{if} \quad 0 < \mathbf{s}(i,j) < mn \end{cases},$$

where $\mathbf{s}(i,j)$ is sum of $\mathbf{Z}'$ at the (i,j) within $m \times n$ window. $0 < \mathbf{s}(i,j) < mn$ means the position (i,j) is on the boundary of focused region.

The proposed method adopts IVC and final map to improve the quality of fused image (selects clear coefficients from wavelet coefficients of source images) and to build up the performance of image edge detection. In this section, a heuristic approach is adopted to take the average of the fused results, which obtained by independent fusion with $\mathbf{\Psi}_{\phi_k}$ for $k = 0, 1, \cdots, R-1$. Our proposed heuristic fusion is simply realized by

$$\mathbf{x}_F = \frac{1}{R}\mathbf{D}^T\mathbf{c}_F = \frac{1}{R}\sum_{k=0}^{R-1} \mathbf{\Psi}_{\phi_k}^T \Theta(\mathbf{\Psi}_{\phi_k}\mathbf{x}_A, \mathbf{\Psi}_{\phi_k}\mathbf{x}_B).$$

4.2 Experimental Results

Through some experiments, we confirm effectiveness of the image fusion method based on M-DirLOTs and IVC.

4.2.1 Performances of Four Transforms

For image fusion in transform domain, there is a problem in the choice of the optimal transform basis for signal representation. Hereon, we use a

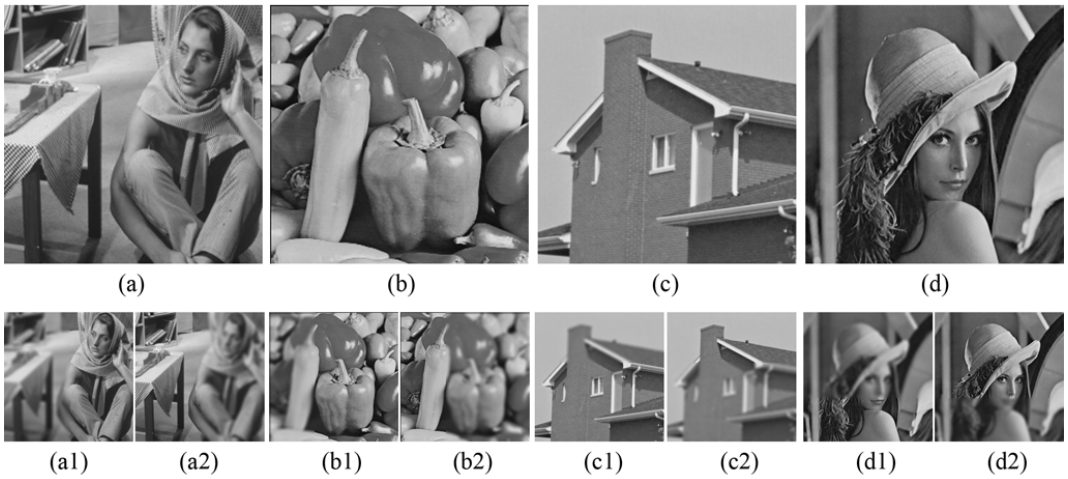

Figure 4.3: Test images of size 256 × 256, 8-bit grayscale and the artificially generated blurred images with different focus levels. (a) Barbara, (b) Peppers, (c) House, (d) Lena.

classical fusion rule (averages low-frequency coefficients and selects absolute maximum of high-frequency coefficients) to evaluate the effect of some existing transforms. Table 4.1 summarizes four transforms and their features. Fig.4.3 shows test images and in the comparison experiment of fusion performance of four transforms which are conducted using artificially generated images with different focus levels. "Barbara," "Peppers," "House" and "Lena," were used, and the sizes of them were all 256 × 256 pixels.

Fig.4.4 shows the magnified regions of "Peppers" and "Lena". Fig.4.5 and Fig.4.6 show some partial results. We can see that M-DirLOTs show better quality for edges, detail informations and gradual changing from figures. The fusion performances were summarized in Table 4.2. Table 4.2 shows that the proposed M-DirLOTs achieved the highest PSNR for all the four images at different focus levels. It can be seen from Table 4.2 that that the proposed M-DirLOTs achieved the highest SSIM (structural similarity), which illustrated that the M-DirLOTs worked well for diagonal edges and textures [42]. As expected, experiments demonstrate that M-DirLOTs outperform other transforms in the same fusion rule.

4.2.2 Comparison of Performances between VC and IVC

We use the above mentioned method to evaluate the effect of IVC. "Pepsi" (512×512), "Disk" (480×640) and "Lab" (480×640) were used. Fig.4.7 shows multi-focus source images. Mutual information (MI) and $Q^{AB/F}$ as information

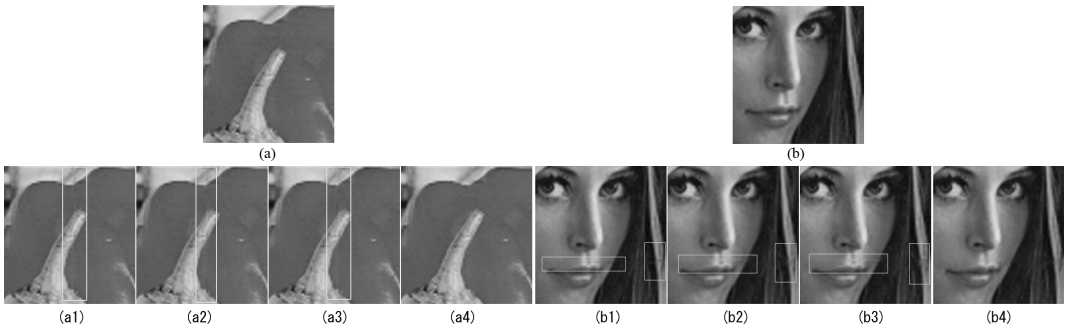

Figure 4.4: Magnified regions of "Peppers" and "Lena". (a) group and (b) group are fused images, where UDHT, NSCT, NSST and M-DirLOTs, respectively.

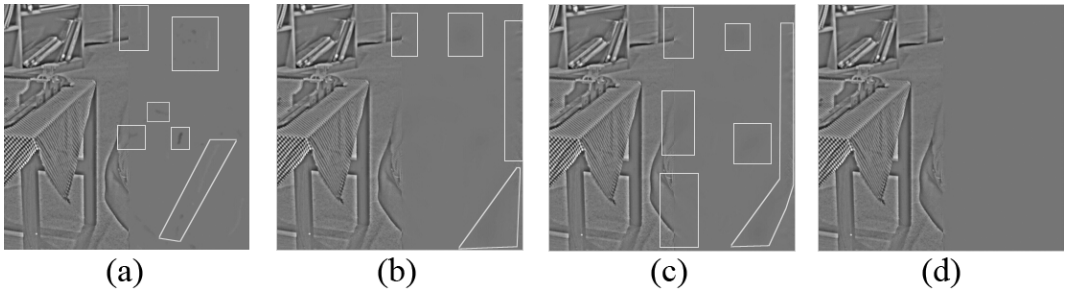

Figure 4.5: Results for "Barbara". (a) ,(b), (c) and (d) are the difference images between fusd result and Fig.4.3(a1), where UDHT, NSCT, NSST and M-DirLOTs, respectively.

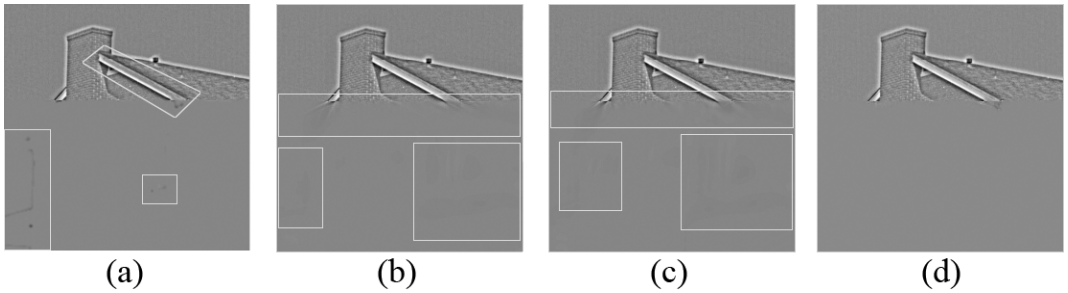

Figure 4.6: Results for "House". (a) ,(b), (c) and (d) are the difference images between fusd result and Fig.4.3(c1), where UDHT, NSCT, NSST and M-DirLOTs, respectively.

Table 4.2: Comparison of PSNRs [dB] and SSIMs among four transforms

	PSNR				SSIM			
Image	Barbara	Peppers	House	Lena	Barbara	Peppers	House	Lena
UDHT	47.97	42.63	45.11	43.43	0.9977	0.9949	0.9980	0.9964
NSCT	47.50	44.22	48.46	44.51	0.9987	0.9973	0.9986	0.9978
NSST	46.62	42.87	47.87	43.88	0.9986	0.9977	0.9986	0.9978
M-DirLOTs	**55.13**	**45.63**	**54.38**	**49.99**	**0.9995**	**0.9985**	**0.9996**	**0.9992**

Table 4.3: Comparison of MI and $Q^{AB/F}$ between VC and IVC without focused regions detection

Image	MI			$Q^{AB/F}$		
	Pepsi	Disk	Lab	Pepsi	Disk	Lab
VC	6.9702	6.2194	**7.3573**	0.7733	0.6865	0.7319
IVC	**6.9764**	**6.2282**	7.3566	**0.7737**	**0.6979**	**0.7328**

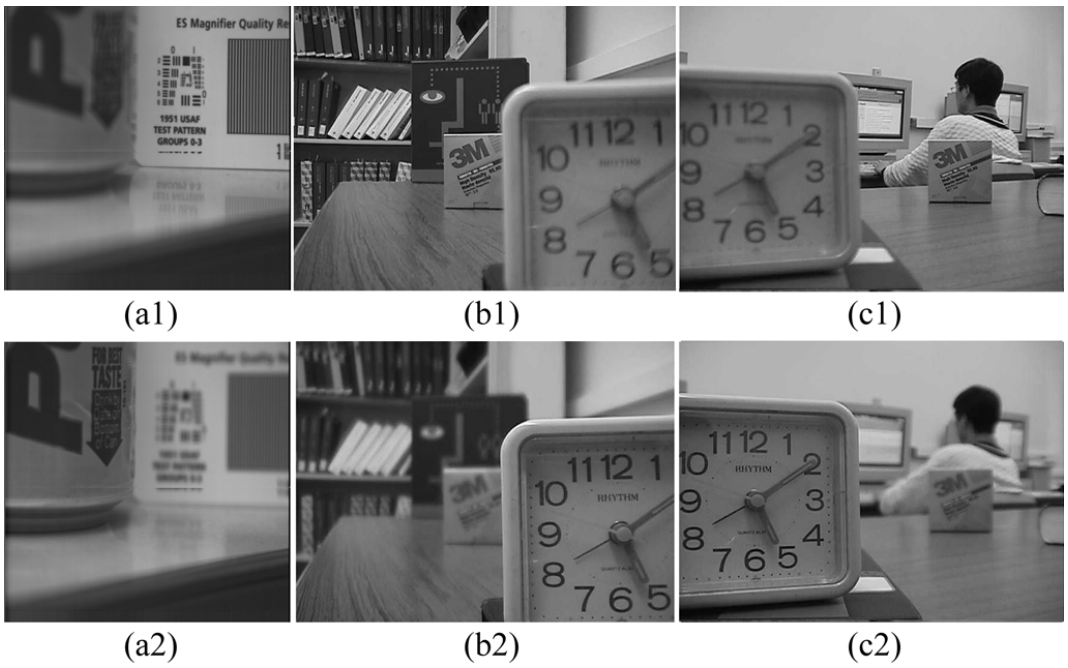

Figure 4.7: Multi-focus source images.

measures for evaluating image fusion performance were used. MI represents how much of the information in the fused image was obtained from the input images [48]. $Q^{AB/F}$ uses Sobel edge detection to measure how much edge information in the fused image can be obtained from the source images [49]. Table 4.3 compares the performances between VC and IVC. It can be seen

that the IVC can achieve highest MI and $Q^{AB/F}$ except the case that the MI of "Lab".

4.2.3 Comparison of MI and $Q^{AB/F}$ among Four Methods

In this experiment, Li's[21], Yong's[23] and Liu's[13] method were used as references. Four decomposition levels, with 4, 8, 8, 16, directions from coarser scale to finer scale, are used in the Li's method. The numbers of hierarchical level of DT-ℂWT was set to 3. Figs.4.8-4.10 show the experimental results. It can be seen that the quality of fused image edges with the proposed method is better than the results of Li's, Yong's and Liu's method. Table 4.4 compares the MI performances and $Q^{AB/F}$ metric among four methods. We can see that the proposed method outperforms the other methods.

The experimental results imply that M-DirLOTs are not only able to reproduce the structure appropriately, but also generate good results. By introducing directional decomposition into the transform, M-DirLOTs can efficiently obtain diagonal components present in natural images.

4.3 Summary

Wavelet-based image fusion methods for multi-focus images were reviewed. It was pointed out that the representation of geometric structures is relatively insufficient by using traditional separable transform. In order to solve this problem, M-DirLOTs was introduced to improve the image fusion quality for edges and textures. Meanwhile, IVC was applied to further the fusion performance. Experimental results show the imageing fused performance was improved, and their effectiveness has been verified.

Table 4.4: Comparison of MI and $Q^{AB/F}$ among four methods

Image	MI			$Q^{AB/F}$		
	Pepsi	Disk	Lab	Pepsi	Disk	Lab
Li's method[21]	8.7862	8.0970	8.6365	0.7916	0.7310	0.7555
Yong's method[23]	8.7141	8.1987	8.4971	0.7851	0.7339	0.7553
Liu's method[13]	8.6289	8.2165	8.5201	0.7885	0.7364	0.7585
Proposed	**8.8728**	**8.2712**	**8.7877**	**0.7939**	**0.7375**	**0.7588**

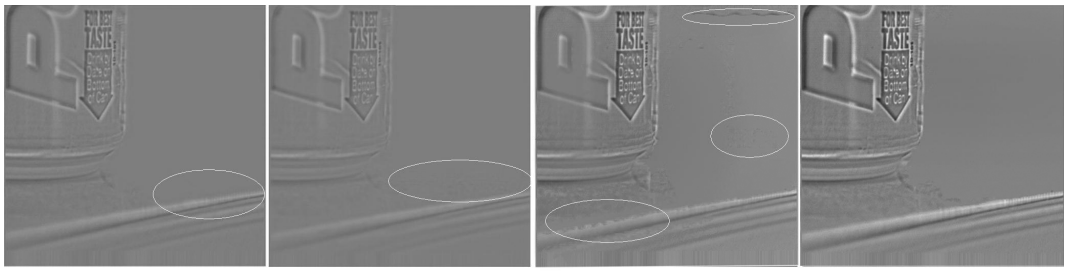

(a) (b) (c) (d)

Figure 4.8: The 'Pepsi' fused images of different methods. (a)-(d) are the difference images between fused images and Fig.4.7(a1), where Li's method, Yong's method, Liu's method and proposed method, respectively.

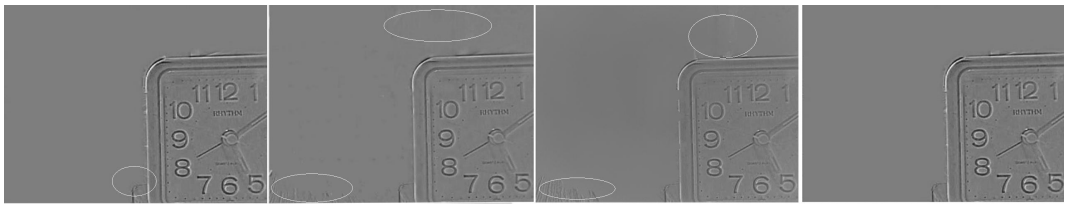

(a) (b) (c) (d)

Figure 4.9: The 'Disk' fused images of different methods. (a)-(d) are the difference images between fused images and Fig.4.7(b1), where Li's method, Yong's method, Liu's method and proposed method, respectively.

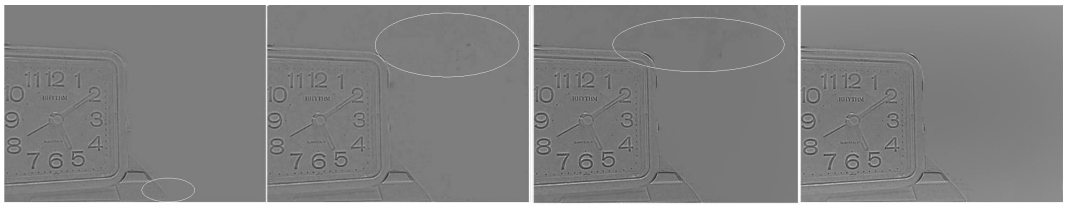

(a) (b) (c) (d)

Figure 4.10: The 'Lab' fused images of different methods. (a)-(d) are the difference images between fused images and Fig.4.7(c1), where Li's method, Yong's method, Liu's method and proposed method, respectively.

5 Conclusions

5.1 Contributions

In this thesis, our aim is to improve the performances for image denoising and image fusion. The traditional multi-scale transforms, DCT, Haar, Symlet, DT-ℂWT, Curvelet, NSCT and NSST are used for the application of image restoration.

It is pointed that the traditional transforms have some disadvantages of representing geometric structures and memory consumption, and there are deficiencies worth mentioning. For traditional separable transforms, they cannot represent slant textures and edges for various directions. For traditional non-separable transforms, they have high computational complexities. Therefore, we have proposed a non-separable directional lapped orthogonal transforms to solve these problems. It has been verified through some experiments that this transform has improved the image representation.

The experimental results suggest that proposed approachs are promising alternative for image restoration. Although our methods are based on maximally decimated directional transform, they output results that are comparable to translation-invariant and undecimated approaches. Simultaneously, our algorithms reduce computational complexity and smaller memory requirement than undecimated transform models. Based on these features, our methods can be applied to obtain high-quality photographs under poor imaging conditions (low-power light source, short exposure time, phototoxicity and signal focus system) in the photon acquisition applications.

The summarizations of each chapters are as follows:

Chapter 2

In Chapter 2, the features of DirLOTs were introduced. From comparison with the traditional transforms, how to choose the transform of the proposed method was explained. The parameters of the M-DirLOTs were determined.

Chapter 3

In Chapter 3, in order to fully improve the quality of image restoration, the state-of-the-art methods are considered in this work. The multi-resolution and multi-directional wavelets are employed in each decomposition level. The SURE-LET approach for Gaussian noise was reviewed as an orthonormal wavelet-based denoising technique. And it can overcome the disadvantage that the representation of diagonal geometric structures is relatively insufficient by using traditional separable transform. Therefore, the classical VST

and one-pass manner SURE-LET are combined to significantly improve the Poisson denoising performance. It was demonstrated experimentally that the proposed Poisson denoising method outperforms some state-of-the-art Poisson denoising algorithms. At the same time, the computational efficiency has been improved significantly too.

Chapter 4

In Chapter 4, the image fusion presented in this thesis is related to the local luminance contrast. In traditional applications, some traditional wavelet transforms have been evolved. But these transforms cannot efficient capture diagonal geometric structures of natural images. Simultaneously, the traditional multiple directional transforms (e.g., NSCT and NSST) cannot satisfy orthogonality, and the computational complexities and redundancy are high. For more effective representation of image, we used a new transform (M-DirLOTs) of representations using non-separable and directional filter banks that can efficiently represent images containing contours, textures and gradation with few coefficients. The local luminance contrast was applied to improve the fusion quality in traditional methods. The local brightness of the background without degradation is needed under the definition of local luminance contrast. Or equivalently, the low-frequency information is more exactly, the authentic local luminance contrast is better. To get the deep low-frequency information, the interscale correlation of wavelet coefficients was used. Therefore, IVC was proposed to fuse high-frequency information. A large number of experiments verify that proposed method can compete and outperform the state-of-the-art fusion methods.

5.2 Open Problems

There remain some problems for the proposed method. In future work, we optimize dictionary for image representation. We can take the geometric structures of images well and reduce memory utilization using the optimized dictionary. Based on the optimized dictionary, the perfermance of image restoration will be further improved. For example, high resolution image Poisson denoing, multi-focus color image fusion and multi-exposure color image fusion. Let us summarize them as open problems.

5.2.1 Dictionary Optimization

From the research in this thesis, we can conclude that some properties of wavelet coefficients are very critical for improving the results of image restoration, which are sparsity, directivity and flexibility.

Sparsity is a description closely related to image compression. In this thesis, we have shown that wavelets can represent image sparsity for various nature images. The image sparse representation means wavelet transform has found the intrinsic structure in the input images. In other words, that means the transform can help with better restoration. For our future work, we have to take into consideration the sparsity.

Directivity is provided by M-DirLOTs. It matches the human visual system, which overcomes the traditional multi-scale transforms. In this thesis, heuristic operation was adopted for image denoising and fusion. However, this approach leads to the loss of some details and the oversmoothness, and the multi-directional properties are not used effectively. Therefore, the choice of the optimal coefficients for signal representation will be concerned.

Flexibility means that M-DirLOTs can be applied in different situations (e.g., denoising, deblurring, super-resolution, inpainting and fusion). In order to improve quality of image restoration in different situations, the choice of the TVM angles need to be considered.

5.2.2 Extensive Application

Mixed Poisson – Gaussian Noise In Chapter 3, an efficient Poisson denoising algorithm was proposed. Recently, high resolution displays are becoming in use in practical appliances, e.g. 8K TV, and medical implements. Consider also an image acquisition system. The system should take a photo which has enough resolution for detecting and analysing objects under inferior conditions. Considering the influence of photon collection, the Poisson noise appear in the photon acquisition system. At the same time, Gaussian noise is possible to occur in an image obtained by digital image acquisition, where the intrinsic thermal and electronic fluctuations of the acquisition devices. The noise corrupted by the two sources mentioned above can be modeled as Poisson-Gaussian noise, where the Poisson component accounts for the signal-dependent uncertainty inherent to photon accumulation, and the Gaussian component accounts for the other signal-independent noise sources, such as thermal noise. A problem lies in estimating the underlying intensity of Poisson noise, potentially further degraded by Gaussian noise.

Adaptive Weight Map Fusion In Chapter 4, one approach based on IVC (averages low-frequency coefficients and selects the either value on corresponding position with maximum of IVC coefficients) was applied. Recent years, the weight construction is proposed to combine pixel saliency and spatial

context for image fusion. In order to obtain pixel saliency and spatial consistency of fused image, the weight map construction need to be considered.

Color Image Restoration In Chapter 3 and Chapter 4, grayscale image restoration approachs were introduced. In a real-world situation, nature images are color. For color image denoising, the psychology of color image perception of human need to be considered. Meanwhile, the multi-focus color image fusion and multi-exposure color image fusion is suitable for human and machine perception or further processing. From these backgrounds, image restoration is demanded in a lot of image and video processing applications. In the future, by further taking the inadequacies of the proposed method such as the color image, we plan to develop more effective fusion rule to overcome the limitations discussed above. Simultaneously, how to improve the effectiveness of the proposed method by adaptively choosing the parameters of the proposed method can be further researched.

References

[1] Alessandro Foi, Sakari Alenius, Mejdi Trimeche, Vladimir Katkovnik, Karen O. Egiazarian, "A spatially adaptive Poissonian image deblurring," *IEEE Proc. ICIP 2007*, pp. 925-928, Sept. 2005.

[2] F. Luisier, C. Vonesch, T. Blu, and M. Unser, "Fast interscale wavelet denoising of Poisson-corrupted images," *Signal Processing*, Vol. 90,No. 2, pp. 415 - 427, Feb. 2010.

[3] Foi, A., "Clipped noisy images: heteroskedastic modeling and practical denoising" *Signal Processing*, vol. 89, no. 12, pp. 2609-2629, Dec. 2009.

[4] P. Fryzlewicz and G.P. Nason, "A Haar-Fisz algorithm for Poisson intensity estimation," *Journal of Computational and Graphical Statistics*, vol. 13, no. 3, pp. 621-638, 2004.

[5] Starck, J. L., F. Murtagh, and A. Bijaoui, "Image Processing and Data Analysis," *Cambridge University Press*, Cambridge, 1998.

[6] F. J. Anscombe, "The transformation of Poisson, binomial and negative binomial data," *Biometrika*, vol. 35, no. 3/4, pp.246-254, 1948.

[7] B. Zhang, J. M. Fadili, and J.-L. Starck, "Wavelets, ridgelets, and curvelets for Poisson noise removal," *IEEE Trans. on Image Processing*, vol. 17, no. 7, pp. 1093-1108, Jul. 2008.

[8] F. Luisier, C. Vonesch, T. Blu, and M. Unser, "A New SURE Approach to Image Denoising: Interscale Orthonormal Wavelet Threshding," *IEEE Trans. on Image Processing*, vol. 16, no. 3, March 2007.

[9] Zhang, B., M.J. Fadili and J.L. Starck, "Multi-Scale Variance Stabilizing Transform for Multi-Dimensional Poisson Count Image Denoising," *IEEE Proc. ICASSP 2006*, vol. 2, pp. 81-84, May. 2006.

[10] Makitalo, M., Foi, A., Alessandro Foi, "A closed-form approximation of the exact unbiased inverse of the Anscombe variance-stabilizing transformation," *IEEE Trans. Image Process*, vol. 20, no. 9, pp. 2697-2698, Sep. 2011.

[11] A. A. Goshtasby, S. Nikolov and Guest editorial, "Image fusion: Advances in the state of the art," *Information Fusion*, vol. 8, pp. 114-118, Apr. 2007.

[12] Veysel Aslantas and Ahmet Nusret Toprak, "A pixel based multi-focus image fusion method," *Optics Communications*, vol. 332, no. 1, pp. 350-358, Dec. 2014.

[13] Yu Liu, Shuping Liu, Zengfu Wang, "Multi-focus image fusion with dense SIFT," *Information Fusion*, vol. 23, no. 1, pp. 139-155, 2015.

[14] H. Li, B. S. Manjunath, S. K. Mitra, "Multisensor image fusion using the wavelet transform," *Graphical Models and Image Processing*, vol. 57, pp. 235-245, May. 1995.

[15] O. Rockinger, "Image sequence fusion using a shift-invariant wavelet transform," *IEEE International Conference on Image Processing*, vol.3, pp. 288 - 291, Oct. 1997.

[16] J. J. Lewis, R. J. O'Callaghan, S. G. Nikolov, D. R. Bull, N. Canagarajah, "Pixel-based and region-based image fusion with complex wavelets," *Information Fusion*, vol. 8, pp. 119-130, Apr. 2007.

[17] Y. Niu, L. Shen, X. Huo and G.Liang, "Multi-objective wavelet-based pixel-level image fusion using multi-objective constriction particle swarm optimization," *Studies in Computational Intelligence*, vol. 261, pp. 151-178, 2010.

[18] Yue Lu and M. N. Do, "A New Contourlet Transform with Sharp Frequency Localization," *IEEE International Conference on Image Processing*, pp. 1629-1632, Oct. 2006.

[19] Qu Xiao Bo, Yan Jing Wen and Yang Gui De, "Sum-modified-Laplacian-based Multifocus Image Fusion Method in Sharp Frequency Localized Contourlet Transform Domain," *Optics and Precision Engineering*, vol. 17, no. 5, pp. 1203-1212, Jun. 2009.

[20] H. Zhao, Z. Shang, Y. Y. Tang, and B. Fang, "Multi-focus image fusion based on the neighbor distance," *Pattern Recognition*, vol. 46, no. 3, pp. 1002-1011, Mar. 2013.

[21] H. Li, Y. Chai, and Z. Li, "Multi-focus image fusion based on nonsubsampled contourlet transform and focused regions detection," *Optik*, vol. 124, no. 1, pp. 40-51, Jan. 2013.

[22] G. Guorong, X. Luping, and F. Dongzhu, "Multi-focus image fusion based on non-subsampled shearlet transform," *IET Image Processing*, vol. 7, no. 6, pp. 633-639, Aug. 2013.

[23] Yong Yang, Song Tong, Shuying Huang, and Pan Lin, "Dual-Tree Complex Wavelet Transform and Image Block Residual-Based Multi-Focus Image Fusion in Visual Sensor Networks," *Sensors*, vol. 14, no.12, pp. 22408-22430, Nov. 2014.

[24] Selesnick, I. W., Baraniuk, R. G. and Kingsbury, N.C., "The dual-tree complex wavelet transform," *IEEE Signal Processing Magazine*, vol. 22, no.6, pp. 123-151, Nov. 2005.

[25] J. Ma and G. Plonka, "The curvlet transform-a review of recent applications," *IEEE Signal Process. Mag.*, vol. 27, no. 2, pp. 118-133, Mar. 2010.

[26] M. N. Do and M. Vetterli, "The contourlet transform: An efficient directional multiresolution image representation," *IEEE Trans. Image Process.*, vol. 14, no. 12, pp. 2091-2106, Dec. 2005.

[27] Cunha, A.L., Zhou, J., Do, M.N., "The non-subsampled contourlet transform: theory, design, and applications," *IEEE Trans. on Image Processing*, vol. 15, no. 10, pp. 3089-3101, Oct. 2006.

[28] Easley, G., Labate, D., Wang, Q.L., "Sparse directional image representations using the discrete shearlet transform," *Appl. Comput.Harmon. Anal.*, vol. 25, no. 1, pp. 25-46, Jul. 2008.

[29] Shogo Muramatsu and Dandan Han, "Image Denoising with Union of Directional Orthonormal DWTs," *IEEE Proc. ICASSP 2012*, pp.1089-1092, Mar. 2012.

[30] S. Muramatsu, D. Han, T. Kobayashi, and H. Kikuchi, "Directional Lapped Orthogonal Transform: Theory and Design," *IEEE Trans. on Image Processing*, vol. 21, no. 5, May 2012.

[31] A. Adachi, S. Muramatsu, and H. Kikuchi, "Constraints of second-order vanishing moments on lattice structures for non-separable orthogonal symmetric wavelets," *IEICE Trans. Fundamentals*, vol. E92-A, no. 3, pp. 788-797, Mar. 2009.

[32] T. Blu and F. Luisier, "The SURE-LET approach to image denoising," *IEEE Trans. Image Process*, vol. 16, no. 11, pp. 2778-2786, Nov. 2007.

[33] M. Elad, "Why simple shrinkage is still relevant for redundant representations," *IEEE Trans. Inf. Theory*, vol. 52, no. 12, pp. 5559-5569, Dec. 2006.

[34] D. L. Donoho and I. M. Johnstone, "Adapting to unknown smoothness via wavelet shrinkage," *J. Amer. Statist. Assoc.*, vol. 90, no. 432, pp. 1200-1224, Dec. 1995.

[35] L. Sendur and I. W. Selesnick, "Bivariate shrinkage with local variance estimation," *IEEE Trans. on Signal Processing Letters*, vol. 9, no. 12, pp. 438-441, Dec. 2002.

[36] NESTA algorithm. http://statweb.stanford.edu/ candes/nesta/.

[37] ST-NLM algorithm. http://www.bioimageanalysis.org/pg-ure/.

[38] PURE-LET algorithm. http://scholar.harvard.edu/fluisier/software/image-denoising.

[39] Raymond H. Chan and Ke Chen,"Multilevel Algorithm for a Poisson Noise Removal Model with Total-variation Regularization," *International Journal of Computer Mathematics*, no.5, pp.1-18, May, 2007.

[40] A. Buades, B. Coll, and J. M. Morel,"A review of image denoising algorithms, with a new one," *Multiscale Model. Simul.*, vol. 4, no. 2, pp. 490-530, 2005.

[41] Le Montagner. Y, Angelini. E. D and Olivo-Marin. J. C,"An Unbiased Risk Estimator for Image Denoising in the Presence of Mixed Poisson-Gaussian Noise," *IEEE Trans. Image Process*, vol. 23, no.3, pp.1255-1268, Mar. 2014.

[42] Z. Wang, A. C. Bovik, H. R. Sheikh, and E. P. Simoncelli, "Image quality assessment: From error visibility to structural similarity," *IEEE Trans. Image Process*, vol. 13, no. 4, pp. 600-612, Apr. 2004.

[43] Zhong Zhang and Rick S. Blum, "A Categorization of Multiscale-decomposition-based Image Fusion Schemes with a Performance Study for a Digital Camera Application," *Proc. of the IEEE*, vol. 87, no. 8, pp.1315-1326, Aug. 1999.

[44] Wei Huang, Zhongliang Jing, "Evaluation of focus measures in multi-focus image fusion," *Pattern Recognition Letters*, vol. 28, no.4, pp. 493-500, Mar. 2007.

[45] A. Toet, L. J. van Ruyven and J. M. Valeton, "Merging Thermal And Visual Images By A Contrast Pyramid," *Optical Engineering*, vol. 28, no. 7, pp. 789-792, Jul. 1989.

[46] A. B. Watson, "Efficiency of a model human image code," *J. Opt. Soc. Am. A*, vol. 4, no. 12, pp. 2401-2417, Dec. 1987.

[47] T. Stathaki, "Image fusion algorithms and applications," *Academic Press is an imprint of Elsevier*, 2008.

[48] P. Viola and W. M. Wells, "Alignment by maximization of mutual information," *International Journal of Computer Vision*, vol. 24, no. 2, pp. 137-154, Sep. 1997.

[49] Vladimir Petrovic and Costas Xydeas, "Objective Image Fusion Performance Characterisation," *Proc. of ICCV'05*, vol. 2, pp. 1866-1871, Oct. 2005.

Biography

Zhiyu Chen graduated from the Yunnan University, Kunming, China, in 2007 and received M.E. degree in electrical and electronic engineering from Niigata University in 2012. He is a currently a Ph.D. candidate at Niigata University. His research interests are in image processing. He is a student member of IEEE(Institute of Electrical and Electronics Engineers, Inc.), and a student member of IEICE(Institute of Electronics, Information and Communication Engineers).

Research Works

Academic Papers

1. Zhiyu CHEN and Shogo MURAMATSU, "SURE-LET Poisson Denoising with Multiple Directional LOTs," IEICE Transactions on Fundamentals, vol.E98-A, no.8, pp. 1820-1828, Aug. 2015.

2. Zhiyu CHEN and Shogo MURAMATSU, "Multi-focus Image Fusion based on Multiple Directional LOTs," IEICE Transactions on Fundamentals, vol.E98-A, no.11, Nov. 2015 (Accepted).

International Conference

1. Zhiyu CHEN and Shogo Muramatsu, "Poisson denoising with multiple Directional LOTs," Proc. of 2014 IEEE International Conference on Acoustics, Speech and Signal Processing (ICASSP), pp.1234-1238, May 2014

Domestic Conferences

1. Zhiyu CHEN and Hisakazu Kikuchi, "Optimized Measurement Matrix for Compressive Sensing Systems," 21st Workshop on Niigata Branch of IEEJ Tokyo Branch, p. 47, Nov. 2011 (In Japanese).

2. Aishan Tuerxun, Zhiyu CHEN and Shogo Muramatsu, "Motion-Compensated Temporal Filtering for Remote Control of Microscope," ITE Technical Report , vol. 37, no. 7, ME2013-23, pp. 87-88, Feb. 2013 (In Japanese).

3. Zhiyu CHEN and Shogo Muramatsu, "Poisson Denoising using Multiple DirLOTs based on Anscombe Transform," 28th IEICE Signal Processing Symp., Nov. 2013 (In Japanese).

4. Zhiyu CHEN and Shogo Muramatsu, "Image Fusion with Multiple Directional LOTs," 29th IEICE Signal Processing Symp., po. 233-236, Nov. 2014 (In Japanese).

5. Takumi Kawamura, Sho Wakasugi, Zhiyu CHEN, Shogo Muramatsu and Samuel Choi, "On Application of NSOLT to 3-D OCT Data Denoising," IEICE Technical Report, vol. 115, no. 22, SIP2015-19, pp. 99-104, May. 2015 (In Japanese).